HYDROTHERMAL CHARACTERIZATION OF METAL FOAM-CLADDED PIN FIN ARRAY HEAT SINK

A THESIS SUBMITTED TO
THE GRADUATE SCHOOL OF NATURAL AND APPLIED SCIENCES
OF
MIDDLE EAST TECHNICAL UNIVERSITY

BY

NURSEL GÜLER

IN PARTIAL FULFILLMENT OF THE REQUIREMENTS
FOR
THE DEGREE OF MASTER OF SCIENCE
IN
MECHANICAL ENGINEERING

APRIL 2024

Approval of the thesis:

HYDROTHERMAL CHARACTERIZATION OF METAL FOAM-CLADDED PIN FIN ARRAY HEAT SINK

submitted by **NURSEL GÜLER** in partial fulfillment of the requirements for the degree of **Master of Science in Mechanical Engineering, Middle East Technical University** by,

Prof. Dr. Naci Emre Altun
Dean, **Graduate School of Natural and Applied Sciences** ________________

Prof. Dr. M. A. Sahir Arıkan
Head of the Department, **Mechanical Engineering** ________________

Assoc. Prof. Dr. Özgür Bayer
Supervisor, **Mechanical Engineering, METU** ________________

Prof. Dr. İsmail Solmaz
Co-Supervisor, **Mechanical Eng., Atatürk University** ________________

Examining Committee Members:

Prof. Dr. Almıla Güvenç Yazıcıoğlu
Mechanical Engineering, METU ________________

Assoc. Prof. Dr. Özgür Bayer
Mechanical Engineering, METU ________________

Assist. Prof. Dr. Altuğ Özçelikkale
Mechanical Engineering, METU ________________

Prof. Dr. İsmail Solmaz
Mechanical Engineering, Atatürk University ________________

Prof. Dr. Murat Köksal
Mechanical Engineering, Hacettepe University ________________

Date: 18.04.2024

I hereby declare that all information in this document has been obtained and presented in accordance with academic rules and ethical conduct. I also declare that, as required by these rules and conduct, I have fully cited and referenced all material and results that are not original to this work.

Name Last name: Nursel Güler

Signature :

ABSTRACT

HYDROTHERMAL CHARACTERIZATION OF METAL FOAM-CLADDED PIN FIN ARRAY HEAT SINK

Güler, Nursel
Master of Science, Mechanical Engineering
Supervisor: Assoc. Prof. Dr. Özgür Bayer
Co-Supervisor: Prof. Dr. İsmail Solmaz

April 2024, 65 pages

The advancement of technology has given rise to a growing demand for effective cooling solutions for electronic components. Heat sinks are commonly used for dissipating heat from electronic components to the environment. Along with the developing technology, the cooling capacity of the heat sinks such as pin fin or plate fin heat sinks has become insufficient. Therefore, a need for advanced cooling methods has emerged. Open-cell metal foams are a fascinating class of materials that combine the structural properties of metals with the unique characteristics of foams. They are lightweight, strong, and have high heat transfer area to volume ratio. The aim of this thesis is investigating the heat transfer performance and pressure drop chraracteristics of a novel geometry by cladding aluminum foam onto the outer surface of pin fins on heat sink. In order to validate the numerical model, series of experiments are conducted. After the validation of the numerical model, a metric which is called as performance evaluation criterion (PEC) is used to compare the performances of different Pores Per Inch (PPI) valued aluminum foams. After validating the numerical model, a parametric analysis is performed to see the effects of different foam cladding thicknesses and porosity on heat transfer performance and pressure drop. All of the studied cases show an enhancement in hydrothermal performance. Among the studied geometries at most 46.5% and at least 37.5% increase in hydrothermal performance compared to the base case is observed.

Keywords: Cooling of Electronic Components, Heat Sinks, Open-Cell Metal Foam, Metal Foam Cladded Pin Fin

ÖZ

METAL KÖPÜK KAPLI PİM KANATÇIK DİZİLİ ISI KUYUSUNUN HİDROTERMAL KARAKTERİZASYONU

Güler, Nursel
Yüksek Lisans, Makina Mühendisliği
Tez Yöneticisi: Doç. Dr. Özgür Bayer
Ortak Tez Yöneticisi: Prof. Dr. İsmail Solmaz

Nisan 2024, 65 sayfa

Teknolojinin ilerlemesi elektronik bileşenler için etkili soğutma çözümlerine yönelik talebin artmasına neden olmuştur. Günümüzde ısı kuyuları genellikle aşırı ısının elektronik bileşenlerden çevreye aktarılması için kullanılır. Gelişen teknoloji ile birlikte iğne ve plaka kanatçıklı ısı kuyularının soğutma kapasitesi yetersiz hale gelmiştir. Bu sebeple yeni bir çözüm ihtiyacı zorunluluğu ortaya çıkmıştır. Açık hücreli metal köpükler, elektronik bileşenlerden salınan aşırı ısıyla başa çıkmak için mükemmel adaylardır. Metal köpükler, metallerin yapısal özelliklerini köpüklerin benzersiz özellikleriyle birleştiren büyüleyici bir malzeme sınıfıdır. Hafif, güçlü ve yüksek ısı transfer alanı/hacim oranına sahiptirler. Bu tezin amacı, pim kanatçık dizili ısı kuyusunu alüminyum köpük kaplayarak ısı transfer performansı ve basınç düşüm özelliklerini incelemektir. Sayısal modelin doğrulanabilmesi için bir dizi deney gerçekleştirilmiştir. Sayısal modelin doğrulanmasının ardından, farklı inç başına düşen por sayısı (PPI) değerlerine sahip alüminyum köpüklerin performanslarını karşılaştırmak için bir performans değerlendirme kriteri (PEC) kullanılmıştır. Sayısal model doğrulandıktan sonra, farklı köpük kaplama kalınlıklarının ve gözenekliliğinin ısı transfer performansı ve basınç düşüşü

üzerindeki etkilerini görmek için parametrik bir analiz gerçekleştirilmiştir. İncelenen durumların tümü hidrotermal performansta bir artış göstermektedir. Ele alınan geometriler arasında hidrotermal performansta baz duruma göre en fazla %46.5 ve en az %37.5 oranında artış gözlenmiştir.

Anahtar Kelimeler: Elektronik Bileşenlerin Soğutulması, Isı Kuyusu, Açık Hücre Metal Köpük, Metal Köpük Kaplı İğne Kanatçık Dizisi

To Hayriş and Hilmigo

ACKNOWLEDGMENTS

I would like to thank my supervisor Assoc. Prof. Dr. Özgür Bayer for his supervision and giving me the chance to have this master’s degree by his guidance. His support, advice, criticism, encouragements, and insight throughout the research was so appreciated.

I would like to thank my co-supervisor Prof. Dr. İsmail Solmaz for his invaluable expertise and guidance.

I would also like to thank Seyedmohsen Baghaei Oskouei and Deniz Alp Yılmaz. Without their support and help, it would not be possible for me to come to this point.

I would like to thank Mr. Mustafa Yalçın for his assistance during the experiments.

I would like to thank my mom, dad, and my brother Yiğit. You were always there for me when I needed it the most. You lifted me up, cheered me up and stood by me as always. Also, thanks to my dear sisters İrem Gizem Aras, Aslı Şen Özel, Bilge Serin, Ebru Aktukmak, Ebru Hilal Şahin and Simge Gümüşer. From all over the world their support and love were always with me. To my work besties, Ilgın Akdemir, Hakan Kavak, Mert Karakaş and Kemal Canpolat for helping and supporting me whenever I need without questioning.

Finally, I would like to thank my husband Kaan Kasal for believing in me even at the times which I didn't believe in myself. Without his continuous support it wouldn't be possible for me to get this degree.

TABLE OF CONTENTS

ABSTRACT v
ÖZ vii
ACKNOWLEDGMENTS x
TABLE OF CONTENTS xi
LIST OF TABLES xiii
LIST OF FIGURES xiv
LIST OF ABBREVIATIONS xvi
LIST OF SYMBOLS xvii
CHAPTERS
1 INTRODUCTION 1
1.1 Cooling Methods 2
1.1.1 Passive Cooling 2
1.1.2 Active Cooling 3
1.2 Pin Fin Heat Sinks (PFHS) 4
1.3 Metal Foam Heat Sinks 5
1.4 Metal Foam Included PFHSs 8
1.5 Motivation and Novelty 10
2 METHODOLOGY 11
2.1 Experimental Work 11
2.1.1 Pin Fin Manufacturing 11

2.1.2 Aluminum Foam Preparing and Properties 14
2.1.3 Foam Cladding onto Pin Fins 17
2.1.4 Experimental Setup 18
2.1.5 Experimental Procedure 23
2.1.6 Investigation of Heat Dissipation to Environment 24
2.1.7 Performance Metrics 26
2.1.8 Uncertainty Analysis 27
2.2 Numerical Study 28
2.2.1 Computational Domain 28
2.2.2 Governing Equations and Boundary Conditions 29
2.2.3 Mesh Independence Study 32
2.2.4 Parametric Study 34
3 RESULTS AND DISCUSSION 37
3.1 Validation of Numerical Models 37
3.1.1 Pin Fin Heat Sink 37
3.1.2 FC-PFHS_Ref and 40 PPI FC-PFHS 38
3.1.3 Flow Regime 40
3.2 Comparison of PFHS and FC-PFHSs with Different PPI Values 42
3.3 Parametric Study Results 44
3.3.1 Local Hot Spot Investigation 49
4 CONCLUSION AND FUTURE WORK 53
REFERENCES 57

LIST OF TABLES

TABLES

Table 2.1 The physical properties of the workpieces.. 15

Table 2.2 Related literature studies for properties of aluminum foam of 20 PPI ... 16

Table 2.3 Related literature studies for properties of aluminum foam of 40 PPI ... 16

Table 2.4 The experiment matrix 23

Table 2.5 Uncertainty values of the measuring devices... 27

Table 2.6 Boundary conditions 32

Table 2.7 The results of the mesh independence study.. 33

Table 2.8 Parametric study matrix 35

LIST OF FIGURES

FIGURES

Figure 1.1 Metal foams, (a) Closed cell [21] and (b) Open cell [22] 6
Figure 2.1 Schematic view of PFHS (dimensions in mm) 12
Figure 2.2 Schematic view of PFHS before foam cladding (dimensions in mm) ... 13
Figure 2.3 Machined PFHSs, (a) 10 mm diameter, (b) 5 mm diameter 13
Figure 2.4 Aluminum foams, (a) 20 PPI, (b) 40 PPI (scale bar length=10 mm)..... 14
Figure 2.5 Schematic view of FC-PFHS (dimensions in mm) 17
Figure 2.6 FC-PFHSs, (a) 20 PPI and (b) 40 PPI 18
Figure 2.7 (a) Experimental setup (b) Enlarged view of inlet channel, heating section and outlet channel 19
Figure 2.8 The fan and inverter device 20
Figure 2.9 Detailed view of the bottom of the heating section 21
Figure 2.10 Anemometer and differential pressure transmitter.............................. 22
Figure 2.11 The heat dissipation for (a) PFHS, (b) 20 PPI FC-PFHS and (c) 40 PPI FC-PFHS 26
Figure 2.12 Computational domain with and without symmetry 29
Figure 2.13 Schematic view of the computational domain and boundaries 31
Figure 2.14 Meshing configurations for (a) PFHS, (b) 20 PPI FC-PFHS............... 33
Figure 2.15 Detailed meshing configuration on symmetry plane for 20 PPI FC-PFHS.. 34
Figure 3.1 Experimental and numerical results for PFHS...................................... 38
Figure 3.2 Experimental and numerical results for FC-PFHS_Ref and 40 PPI FC-PFHS.. 39
Figure 3.3 The velocity and temperature contours for (a) PFHS with D_{PF}=10mm (b) FC-PFHS_Ref, (c) 40PPI FC-PFHS 42
Figure 3.4 Nu for FC-PFHS_Ref, 40 PPI FC-PFHS and PFHS............................. 42
Figure 3.5 PEC of FC-PFHS_Ref and 40 PPI FC-PFHS 43
Figure 3.6 ΔP and Nu of parametric study cases 46

Figure 3.7 Velocity and temperature profile for (a) FC-PFHS_Ref,
(b) FC-PFHS_Case4, (c) FC-PFHS_Case8 48
Figure 3.8 PEC values for the parametric study 49
Figure 3.9 Local temperature distribution of base plate for (a) FC-PFHS_Ref,
(b) FC-PFHS_Case4 and (c) FC-PFHS_Case8... 50

LIST OF ABBREVIATIONS

ABBREVIATIONS

CNC	Computer numerical control
FC-PFHS	Foam cladded pin fin heat sink
FVM	Finite volume method
LTE	Local thermal equilibrium
PEC	Performance evaluation criterion
PFHS	Pin fin heat sink
PPI	Pores per inch
TCR	Thermal contact resistance

LIST OF SYMBOLS

SYMBOLS

k	Conductivity, W/mK
ρ	Density, kg/m^3
D	Diameter, m
μ	Dynamic viscosity, kg/ms
q''	Heat flux, W/m^2
C_F	Inertial coefficient
Nu	Nusselt number ($Nu = hD/k$)
K_F	Permeability, m^2
ε	Porosity
P	Pressure, Pa
ΔP	Pressure drop, Pa
Re	Reynolds number, ($Re = \rho UD/\mu$)
c_p	Specific heat capacity, kJ/kgK
T	Temperature, °C
U	Velocity, m/s
V	Volume, m^3

SUBSCRIPTS

Al	Aluminum
AF	Aluminum foam
eff	Effective
env	Environment
h	Hydraulic
i	Inlet
max	Maximum
PF	Pin fin
p	Porous
supp	Supplied

CHAPTER 1

INTRODUCTION

In an era defined by rapid technological advancement and widespread utilization of digital technology, electronic components stand as the cornerstone of modern civilization. The precedented pace has led to the development of increasingly sophisticated and powerful electronic devices that have become an inseparable part of our daily lives. From the palm-sized smartphones that connect us to the world, to the data centers that drive the digital infrastructure, these electronic devices have redefined the boundaries of human capabilities [1].

With the improvement of technology, a critical concern has emerged which is the need for effective cooling solutions. The escalating demand for processing power, coupled with the shrinking size of components, has led to the generation of substantial heat within these devices [2,3]. This heat, if not adequately managed, has the potential to damage the electronic component. Pedram and Nazarian [4] in their paper states that thermal problems are the main reason or over 50% failures observed in integrated circuits.

To manage this excess heat, using conventional heat sinks for cooling becomes insufficient. At this point, heat sinks produced using open-cell metal foam have begun to be used as a good alternative with their lightweight, high surface area/volume ratio and high flow mixing capability [5]. However, metal foams have lower effective thermal conductivity (k_{eff}) compared to their bulk form, which creates a significant disadvantage in heat transfer applications. Therefore, metal foams are mostly integrated into conventional heat sinks.

In this thesis, a novel heat sink is manufactured. The heat sink consists of eight pin fins with staggered orientation and aluminum foam is cladded onto these pin fins. Hydrothermal characterization of aluminum foam cladded pin fin heat sink (FC-PFHS) for two different pores per inch (PPI) value is studied experimentally. Then numerical model is validated with experimental results and eventually, a parametric study is conducted in order to see the design extends.

1.1 Cooling Methods

1.1.1 Passive Cooling

This technique relies on the principles of thermodynamics and natural convection to dissipate heat without the need for mechanical components. Passive cooling methods can be utilized for low heat flux applications. Since this method doesn’t require a mechanical component, there will be no noise resulted from it and also the cost will be low [5]. Heat sinks, phase change materials and radiative cooling are examples of passive cooling methods.

Heat sinks are passive cooling devices which are made of thermally conductive materials such as aluminum or copper. They are designed with fins or other structures to increase the surface area available for heat dissipation. Heat sinks transfer heat from a hot surface to the surrounding air through convection [6,7].

Phase change materials (PCMs) absorb and release heat during phase transitions, such as melting and freezing, at specific temperatures. They are often used to store thermal energy and maintain consistent temperatures within a system. Common applications include building insulation and thermal management in electronics [8].

Radiative cooling as a passive cooling technique leverages materials with high infrared emissivity to radiate heat away from surfaces to the atmosphere. Radiative cooling is particularly effective during nighttime when the surroundings are cooler than the emitting surface [9].

1.1.2 Active Cooling

Active cooling is a technique which utilizes mechanical components such as pumps, fans, or other devices to remove heat from a system. When natural convection alone is insufficient for adequately cooling a system or component, active cooling systems become necessary. Natural convection relies on the natural movement of air due to density differences caused by temperature variations, but it may not provide enough airflow to dissipate heat efficiently, especially in systems with high heat loads or limited airflow. By utilizing active cooling techniques, systems can effectively manage heat dissipation, prevent overheating, and maintain optimal operating temperatures, ensuring reliable performance and longevity of components [1,5]. The active cooling system can be classified into forced air cooling, liquid cooling and liquid evaporation.

When free convection is not enough, small fans or blowers are commonly used to provide forced air cooling for electronic components. This method is well established, commonly used for data center cooling, reliable and simple in design. Since there exists a fan or blower, noise can occur in the system. They are often attached to heat sinks or directly to the components themselves. Fans increase the airflow around the components, enhancing heat transfer and improving cooling efficiency [10].

Liquid cooling systems use a pump to circulate coolant through channels or cold plates attached to the electronic components. The coolant absorbs heat from the components and carries it away to a radiator or heat exchanger where it is dissipated into the surrounding environment. Liquid cooling is particularly effective for high-power components where air cooling may be insufficient [11,12].

In liquid evaporation, heat is applied to a coolant and liquid coolant becomes vapor then the latent heat of the fluid can be used for cooling. This method provides the highest heat transfer among other methods and therefore is not suitable for small devices. Since it requires heating, installation, maintenance operating costs are higher compared to the rest of the cooling methods.

1.2 Pin Fin Heat Sinks (PFHS)

Heat sinks are used for dissipating excess amount of heat from a heat generating surface to the ambient. Pin-fin heat sinks (PFHSs) are one of the most frequently employed types of heat sinks. PFHSs may have different shapes such as, cylindrical, elliptical, triangular, and square [13]. PFHSs dissipate heat generated by electronic components, such as processors, transistors, or integrated circuits to the ambient. They prevent overheating and ensure optimal performance and reliability.

To characterize pin fins, extensive research has delved into understanding the parameters influencing the hydrothermal performance of these structures. Investigations have been conducted on a range of factors, including the height-to-diameter ratio of the pin fins, the specific shape of the pins, dimensions in both the spanwise and streamwise directions, the arrangement of the pins, and the operating conditions involving both natural and forced convection [14].

Metzger et. al. [15] studied the effects of the shape of the fin and the array orientation on heat transfer performance and pressure drop (ΔP) characteristics. The authors found out that oblong PFHSs increased the heat transfer rate by 20% compared to the circular pin fins. They have also stated that for circular pin fins, orientation with respect to the flow direction has a significant effect on both heat transfer and pressure drop.

Chapman et al. [16] and Khan et al. [17] conducted experimental research to assess the thermal performance of pin fin heat sinks with square, circular, and elliptical cross-sections. Their findings revealed that, in forced convection, pin fins with elliptical cross-sections outperformed their square and circular counterparts in terms of air-side performance.

Jonsson and Bjorn [18] also conducted experimental research on the thermal performance of heat sinks with various fin designs, such as straight fins and pin fins with circular, square, and elliptical cross-sections. The evaluation of thermal performance involved comparing the thermal resistance of these heat sinks with equal average velocity and equal pressure drop. They have found that the use of elliptical pin fins for high velocities and circular pin fins for mid-range velocities are recommended.

Chyu [19] experimentally investigated the effects of arrangement of the pin fins on heat transfer performance and pressure drop. The author concluded that staggered arrangement exhibits better heat transfer performance than in line arrangement but at the expense of high pressure drop.

The analysis of PFHSs extends beyond the fin geometry, encompassing a comprehensive study of various airflow patterns and their corresponding effects.

Issa and Ortega [20] conducted experimental research to explore the thermal and hydraulic characteristics resulting from jet impingement on pin-fin heat sinks. The finding of this investigation revealed that as pin density and pin diameter increased, the pressure loss coefficient also increased. On the other hand, the pressure loss coefficient decreased with higher pin height and clearance ratio.

There had been a notable improvement in enhancing the performance of PFHSs. However, the growing demands driven by technological advancements necessitated the search for a new material.

1.3 Metal Foam Heat Sinks

The need for better cooling solutions started a quest for better heat transfer performance heat sinks. Therefore, instead of modifying the orientation or changing the shapes of the conventional heat sinks, a better way of cooling the electronic components has been found.

Metal foams are porous materials with a high surface area to volume ratio, and this makes them a great candidate for excess heat dissipation. Metal foams can be categorized as open cell and closed cell. If all the pores are connected to each other these types of foams are called open cells and if the cells are separated by walls or there is a gas inside them then these types of foams are called as closed cell. Open cell and closed cell metal foams are depicted in Figure 1.1.

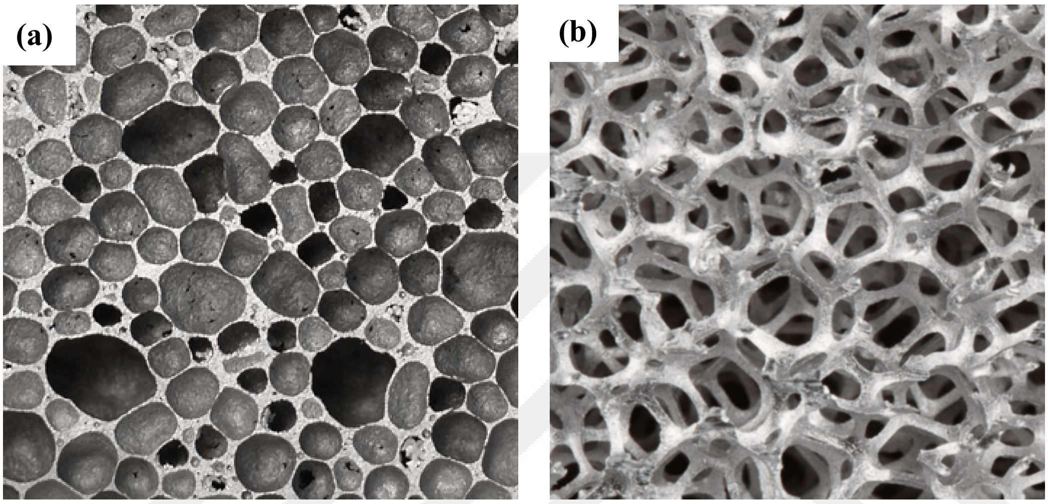

Figure 1.1 Metal foams, (a) Closed cell [21] and (b) Open cell [22]

Calmidi and Mahajan [23] have performed series of experiments by using air and water as working fluids to predict the effective thermal conductivity of metal foams. The authors aimed to increase the usage of metal foams by estimating their thermal conductivity.

Zhao et. al. [24] studied with 12 different metal foams with a range of pore sizes and porosities (ε) both experimentally and numerically. Experiments are conducted for the pressure drop and heat transfer performances. They concluded that cell size has a greater effect than porosity in terms of heat transfer. And an optimal porosity value is achieved for an optimal heat transfer and pressure drop value.

Hsieh et. al. [25] experimentally investigated the heat transfer performances of aluminum foams with different PPI value and porosity. A correlation between the

Nusselt number (Nu) and the Reynolds number (Re) has also been achieved. The experimental results showed that high porosity and high PPI value increases the Nu.

Likewise, Kurtbas and Celik [26] performed experiments on a horizontal channel with different aspect ratios and different PPI values of aluminum foam. The authors concluded that as the PPI value increases, the average Nu increases. The authors also observed that the Nu is proportional to the aspect ratio.

Tamayol and Hooman [27] studied forced convection flow to a metal foam heat exchanger theoretically. The authors have created a model which can be used for deciding the key parameters on overall heat transfer coefficient. It is stated that foams with higher PPI value result in higher heat transfer rates. However, foams with high porosity have lower heat transfer rates with lower pressure drop.

Mancin et. al. [28] experimentally investigated the aluminum and copper foams with different porosity, foam core height and PPI values. The authors concluded that copper foam shows better heat transfer performance than aluminum foam. For the same porosity valued foams, 40 mm high foam did not show a superior heat transfer performance even though its surface area is twice as the 20 mm high foams. 20 mm high foams showed higher hydrothermal performance than 40 mm high foam.

Metal foams have indeed showcased remarkable improvements in heat transfer performance, yet their application as standalone heat sinks faced a challenge with elevated pressure drops, necessitating substantial pumping powers. Relying solely on metal foams as heat sinks didn't emerge as a viable solution for achieving high-efficiency cooling. To capitalize on the exceptional features of metal foams and sustain optimal system performance, the integration of pin fin heat sinks is introduced in conjunction with the use of metal foams. This strategic combination not only uses the exceptional characteristics of metal foams but also ensures effective heat dissipation, thereby enhancing overall cooling efficiency.

1.4 Metal Foam Included PFHSs

Usage of metal foams brings great advantage of high surface area and high flow mixing capacity but the effective thermal conductivity of them is significantly low compared to the bulk aluminum. As a result, it negatively affects the conduction heat transfer rate perpendicular to the flow, causing substantial thermal gradients and consequently, the heat sink's efficiency decreases. Therefore, to eliminate this effect, using metal foams together with the conventional pin fins emerges as a promising solution for optimizing heat transfer performance.

Bhattacharya and Mahajan [29] conducted series of experiments with different PPI aluminum foams and different number of fins. The authors stated that including fins to the foams increases the heat transfer. The thermal performance of the finned metal foam heat sinks is better than conventional finned heat sink by a factor of 1.5 and better than metal foam heat sinks by a factor of 2.

Seyf and Layeghi [30] conducted a numerical analysis for an elliptical PFHS with and without aluminum foam with different porosities and permeabilities (K_F) to observe the heat transfer performance and pressure drop. The results showed that Nu for the aluminum foam included pin fin is higher. Increasing porosity resulted in a decrease in Nu while low K_F results in high pressure drop. The authors suggested that one needs to be careful about selecting the foam for the best hydrothermal efficiency.

Feng et. al. [31] broadly compared the performance of metal foam heat sinks and finned metal foam heat sinks. The authors have conducted a series of experiments with heat sinks of different heights. The results showed that with a constant power, the heat transfer performance of finned metal foam heat sinks are 1.5-2.8 times higher than the metal foam heat sinks. For constant power, heat transfer performance for the metal foam did not change with the height while for the finned metal foam heat sink heat transfer performance increased with the height.

Mohammadian and Zhang [32] studied five different cases in order to investigate the aluminum foam usage inside a battery pack. The authors found that using aluminum foams as pin fins or directly embedding it to the channel didn’t increase the heat transfer rate for thermal management. But the combination of aluminum foam with aluminum pin fins is determined to be a better option for thermal management.

Li et al. [33] proposed a metal foam together with pin fins. The authors introduced thermal contact resistance and observed its effects. They concluded that thermal performance ratio of metal foam together with pin is 1.6 times higher than conventional one. In another research the same authors [34] compared the performance of aluminum foam heat sink and aluminum foam heat sink together with pin fins. The authors found that thermal performance of aluminum foams together with pin fins is 1.5 times that of aluminum foams alone with the same pumping power.

Wang et al [35] conducted an experiment to observe the heat transfer and flow characteristics of three copper foam heat sinks with fins under impingement flow. The authors showed that inserting copper foam increases thermal performance and concluded that the performance of foamed heat sinks is always better than conventional heat sinks with the same pumping power. They also stated that the heat transfer enhancement is better for lower heights and higher PPI.

Ranjbar et. al. [36] conducted a numerical study with five different porous fin geometries which are increasing, decreasing, V-shaped, rectangular and wedge shaped. The authors studied the effect of the arrangement of the pin fins. In order to compare the performance of heat sinks, PEC is used. The authors concluded that decreased and in line pin fin configuration gives the best hydrothermal performance among the studied cases.

Panse et al. [37] aimed to develop different foam-based cooling options. The authors have used 5, 20 and 40 PPI Al foams. They concluded that increasing pore density also increases the heat transfer and pressure drop. The authors also stated that 40 PPI foam resulted in the highest heat transfer rate.

Among all of the studies in literature, the different design options of heat sinks with foams are limited. The prevailing studies primarily focus on two main approaches: either utilizing metal foams as standalone heat sinks or integrating fins into the structure of metal foams.

1.5 Motivation and Novelty

This thesis investigates a novel geometric approach that has not been previously explored. While existing literature typically integrates metal foams into conventional pin or plate fins. It has been observed that these structures often result in a considerable pressure drop, consequently necessitating high pumping powers [29,38]. Therefore, this study diverges from conventional approaches by seeking to enhance the thermal performance of traditional PFHSs without inducing a significant pressure drop.

The methodology involves cladding metal foams onto the outer surface of the pin fins on a heat sink to improve heat transfer rates while maintaining a manageable pressure drop. This approach aims to increase the hydrothermal efficiency of heat sinks.

In order to study the hydrothermal performance, initially, an experimental series will be conducted using PFHS and FC-PFHS with varying PPI values. Subsequently, a numerical model will be developed and validated using the experimental data. Once validated, the numerical model will be employed to identify the FC-PFHS with the most favorable hydrothermal performance. Finally, utilizing the validated numerical model, a parametric study will be carried out on the selected FC-PFHS to determine the parameters influencing its hydrothermal performance.

CHAPTER 2

METHODOLOGY

2.1 Experimental Work

In order to investigate the hydrothermal behavior of PFHSs with or without cladding and validate the numerical model, a series of experiments have been conducted. Two different geometries have been involved in the investigation. The first geometry is a PFHS with 8 pin fins in staggered orientation, each of 10 mm diameter while the second one is FC-PFHS with 5 mm pin fin diameter and two hollow cylinder-shaped aluminum foams of 2.5 mm thickness are cladded onto the outer surfaces of these pin fins. Two different aluminum foams with 20 PPI and 40 PPI value have been used in the experiments.

2.1.1 Pin Fin Manufacturing

In order to investigate the effect of cladding the metal foams on PFHS, firstly, a conventional 6061 aluminum PFHS with 167 W/mK thermal conductivity [39] is manufacutered by computer numerical control (CNC) machining. The heat sink is designed in staggered orientation since in literature there are many studies which show that staggered arrangement has advantages on in-line arrangement [40,41]. Şahin et al. [38] studied the performance of in-line and staggered arrangement pin fins both numerically and experimentally. They have concluded that, although staggered arrangement has less number of pin fins, the in-line arrangement did not show any superiority in terms of heat transfer enhancement and pressure drop characteristics.

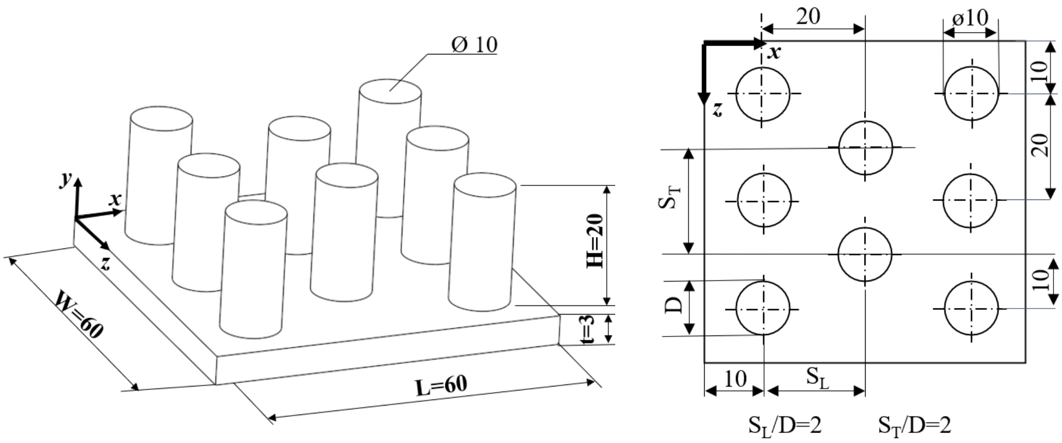

Figure 2.1 Schematic view of PFHS (dimensions in mm)

The heat sink consists of 8 pin fins in staggered orientation with 10 mm diameter and 20 mm height. The dimension of the base plate is 60x60x3 mm. The detailed dimensions of the manufactured heat sink is provided in Figure 2.1.

In literature, the optimal spanwise (S_T/D) and streamwise (S_L/D) spacings and the fin diameter to fin height ratio have been studied extensively [15,42,43]. Chyu et al. [43] stated that for staggered pin fins, a ratio of pin height to diameter value of 2 gives the best heat transfer performance. While Sara [44] stated that if the ratio of fin spacing to diameter decreases, a better heat transfer performance is established.

The geometrical design parameters utilized in this thesis are based on the findings of these prior studies.

In order to clad aluminum foams onto the outer surface of the pin fins, initially two identical heat sinks with 8 pin fins of 5 mm diameter in staggered orientation and 20 mm height have been manufactured. The dimension of the base plate is kept as 60x60x3 mm. The detailed dimensions of the manufactured heat sink are provided in Figure 2.2.

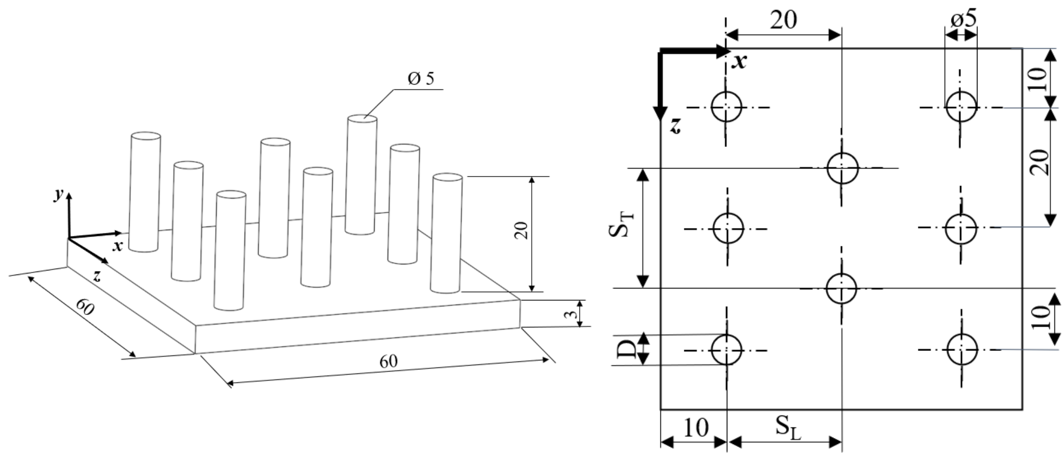

Figure 2.2 Schematic view of PFHS before foam cladding (dimensions in mm)

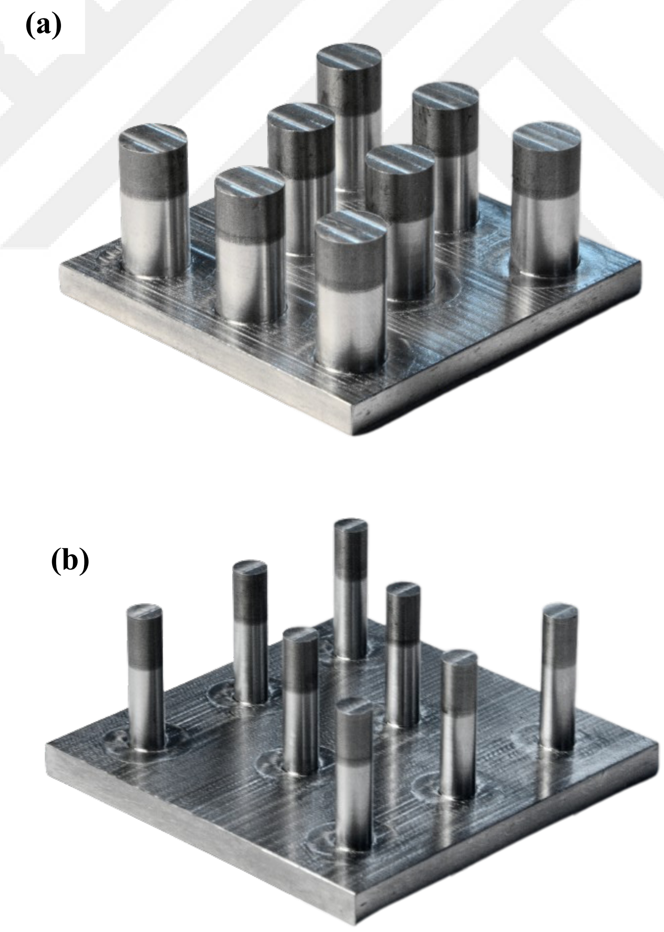

Figure 2.3 Machined PFHSs, (a) 10 mm diameter, (b) 5 mm diameter

For the experiments, the aluminum foams are cladded onto the outer surface of pin fins on heat sinks. For the experimental study, the thickness of the aluminum foam cladding is determined to ensure that the outer diameter of the pin fins remains identical for all heat sinks studied. The machined PFHSs are provided in Figure 2.3.

2.1.2 Aluminum Foam Preparing and Properties

This study utilizes two aluminum foams with distinct PPI values: 20 PPI and 40 PPI. The selection of these two PPI values enables an exploration of their respective impacts on heat transfer performance and pressure drop characteristics. The foams are supplied from ERG Aerospace (Duocel) [45]. The unmachined foams are depicted in Figure 2.4.

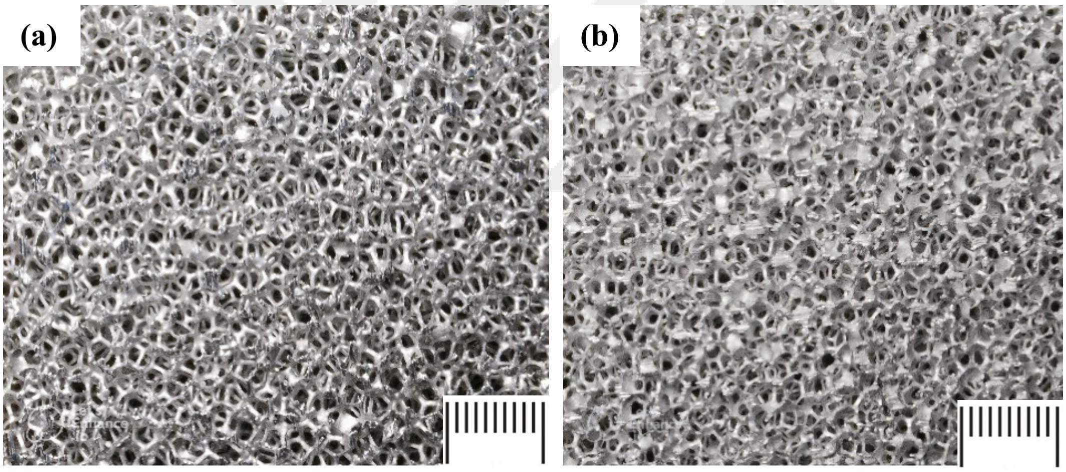

Figure 2.4 Aluminum foams, (a) 20 PPI, (b) 40 PPI (scale bar length=10 mm)

The manufacturer of the aluminum foams does not supply the porosity information directly. Therefore, the ε value of the aluminum foams needed to be evaluated. The ε is defined by the ratio of the void volume (V_{void}) to the total volume (V_{total}) of the aluminum foam as given in Eqn. (2.1) [46].

$$\varepsilon = \frac{V_{void}}{V_{total}} \tag{2.1}$$

Firstly, the aluminum foams are weighed with Radwag AS 60/220.R2 device. Then with the mass information, the aluminum volume of the foams is calculated so that the void volume of the foams can be deducted.

The physical properties of the aluminum foams are provided in Table 2.1.

Table 2.1 The physical properties of the workpieces

	PPI	**Density (kg/m^3)**	**Mass (kg)**	**Total Volume (m^3)**	**Void Volume (m^3)**	**Porosity**
Foam1	20	2700	0.017178	0.000147	0.000141	0.956860
Foam2	40	2700	0.018836	0.000147	0.000140	0.952697

To establish the numerical model, the k_{eff}, K_F, and inertial coefficient (C_F) values are essential. While conducting a series of experiments is one approach to determine these values, the extensive research conducted on ERG aerospace aluminum foams in existing literature provides an alternative source. It is feasible to obtain these values from previous literature works.

Calmidi and Mahajan [47] conducted a study on aluminum foam with a porosity value of 0.9546 to determine its K_F, C_F and k_{eff} values. The porosity value of the 20 PPI aluminum foam in this thesis is 0.9568, which closely aligns with the value from Calmidi and Mahajan's work. Thus, leveraging the thermophysical properties established by Calmidi and Mahajan for the studied aluminum foam appears feasible. For 40 PPI, the porosity value of the aluminum foam is 0.9527. Phanikumar and Mahajan [48] have studied the thermophysical properties of aluminum foam with a porosity value of 0.9586. Likewise, the thermophysical properties established by Phanikumar and Mahajan for 40 PPI aluminum foam can be utilized.

Table 2.2 Related literature studies for properties of aluminum foam of 20 PPI

ε	$K_F \times 10^8$ (m^2)	C_F	k_{eff} (W/mK)	References
0.9	3.12	0.0105	5.1	Leong and Jin [49]
0.93	5.31	0.020	-	Jeng and Tzeng [50]
0.9546	13.00	0.093	3.735	Calmidi and Mahajan [47]
0.9005	9.00	0.088	7.213	Calmidi and Mahajan[47]
0.932	8.24	0.065	-	Mancin et al. [28]
0.93	5.35	0.0498	-	Mancin et al. [28]
0.92	10.60	0.1023	3.130	Phanikumar and Mahajan [48]
0.9353	11.70	0.0982	4.963	Phanikumar and Mahajan [48]

The selected values for K_F, C_F and k_{eff} are highlighted for 20 and 40 PPI in Table 2.2 and Table 2.3, respectively.

Table 2.3 Related literature studies for properties of aluminum foam of 40 PPI

ε	$K_F \times 10^8$ (m^2)	C_F	k_{eff} (W/mK)	References
0.93	2. 71	0.020	-	Jeng and Tzeng[50]
0.9	2.80	0.0155	5.9	Leong and Jin [49]
0.9586	5.98	0.09126	3.385	Phanikumar and Mahajan [48]
0.9272	6.10	0.089	5.504	Calmidi and Mahajan [47]
0.9132	5. 30	0.084	6.607	Calmidi and Mahajan [47]
0.926	2.97	0.0503	-	Mancin et al. [28]
0.93	6.34	0.086	-	Mancin et al. [28]
0.93	4.79	0.076	-	Cavallini et al. [51]
0.9091	5.06	0.08254	6.963	Phanikumar and Mahajan [48]

2.1.3 Foam Cladding onto Pin Fins

For the ease of the assembly aluminum foams have been cut into hollow cylinders. The foams are brought to the desired shape by wire erosion method. Wire erosion is a method to cut a workpiece precisely by using the electrical sparks between the workpiece and the wire [52]. The detailed dimensions of the FC-PFHS are provided in Figure 2.5.

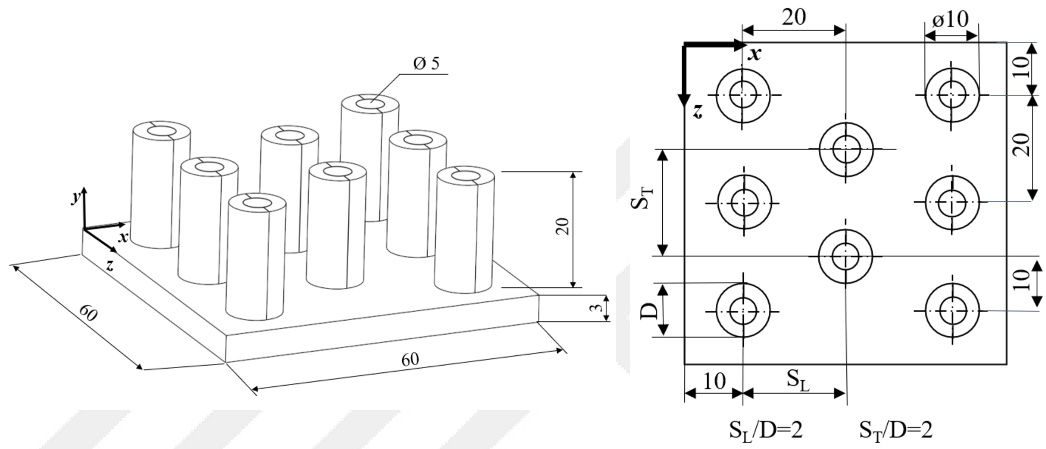

Figure 2.5 Schematic view of FC-PFHS (dimensions in mm)

Then by using EPO-TEK H20E silver epoxy [52], the aluminum foams are cladded onto the outer surface of the pin fins on heatsinks. After the application of the epoxy, according to the instructions provided by the manufacturer, it has been cured at 150 °C for 1 hour.

During the curing process, aluminum foams are secured onto pin fins using copper straps. This ensures proper cladding of the aluminum foams and minimizes contact resistance between the aluminum foam and pin fins. Figure 2.6 illustrates the heat sinks after the aluminum foam cladding operation.

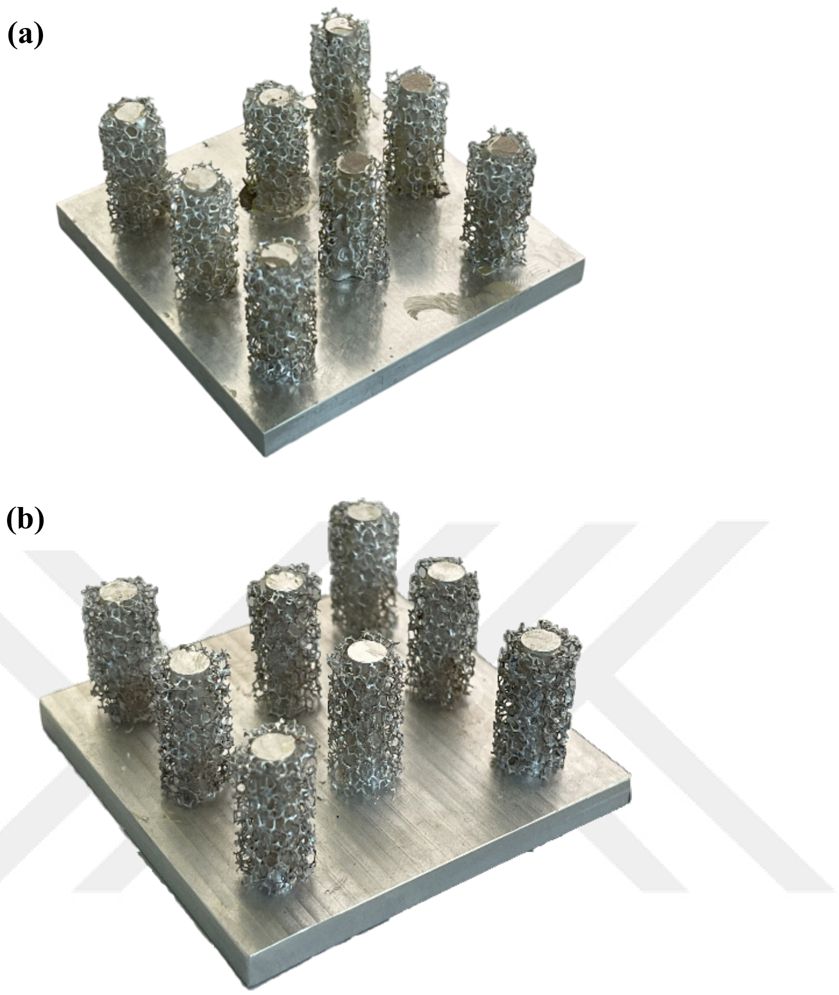

Figure 2.6 FC-PFHSs, (a) 20 PPI and (b) 40 PPI

2.1.4 Experimental Setup

An experimental setup is designed and constructed for the pressure drop measurements and to determine heat transfer characteristics of the manufactured heat sinks. The experimental setup is provided in Figure 2.7 (a). The experimental setup comprises an inlet channel (marked as 1) constructed from plexiglass, measuring 60 cm in length, and an outlet channel (2) with a length of 30 cm.

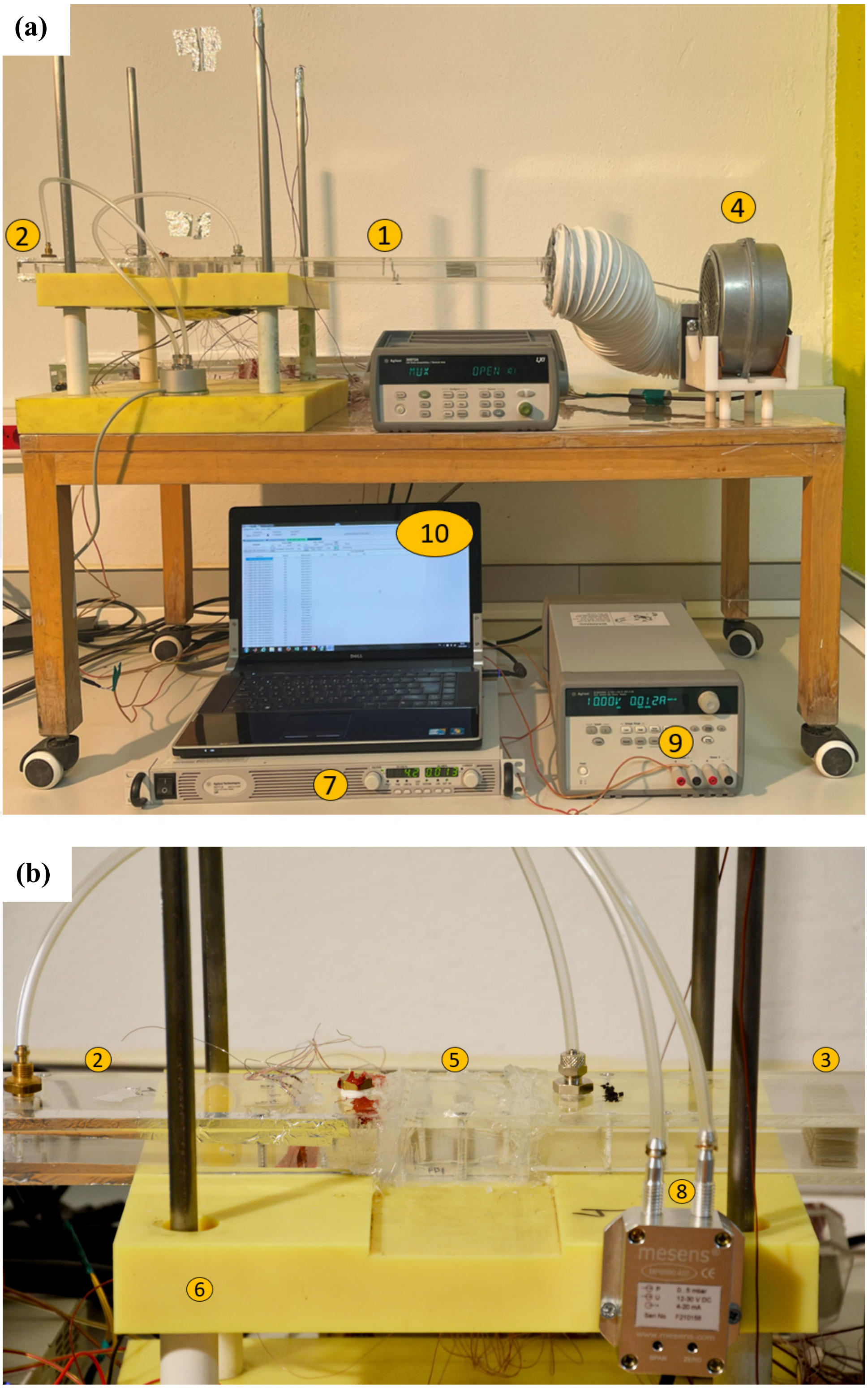

Figure 2.7 (a) Experimental setup (b) Enlarged view of inlet channel, heating section and outlet channel

To ensure uniform airflow, three honeycomb structures (3) are carefully positioned within the inlet channel. The enlarged view of the inlet channel, heating section and outlet channel is provided in Figure 2.7 (b). The inlet channel is linked to an Ebmpapst R2E120-AR77-05 fan (4), with its frequency regulated by a Siemens Sinamics V20 inverter device. The fan and the inverter device used in the experiment are provided in Figure 2.8.

Figure 2.8 The fan and inverter device

The inlet channel is tied to the heating section (5) which consists of the heat sink. The detailed view of the heating section can be depicted in Figure 2.9. Thermal paste with a thermal conductivity of 8 W/mK is applied to the bottom of the heat sink which adheres the heatsink to the 1 mm copper plate. The copper plate is used for the uniform and constant heat transfer from film heater. 15 T-type thermocouples are fixed by aluminum tapes to the bottom surface of the copper plate to measure and register the average temperature of the heatsink. Under the copper plate there exists a thermal pad which is used for eliminating thermal contact resistance between the film heater and the copper plate and for uniform heat transfer. The thermal pad has a thickness of 3 mm, and its thermal conductivity value is 1 W/mK. Under the thermal pad, there exists a film heater with 4.3 Ω resistance value. Beneath the heating section lies a cestamite layer (6) with a very low thermal conductivity, effectively preventing heat dissipation.

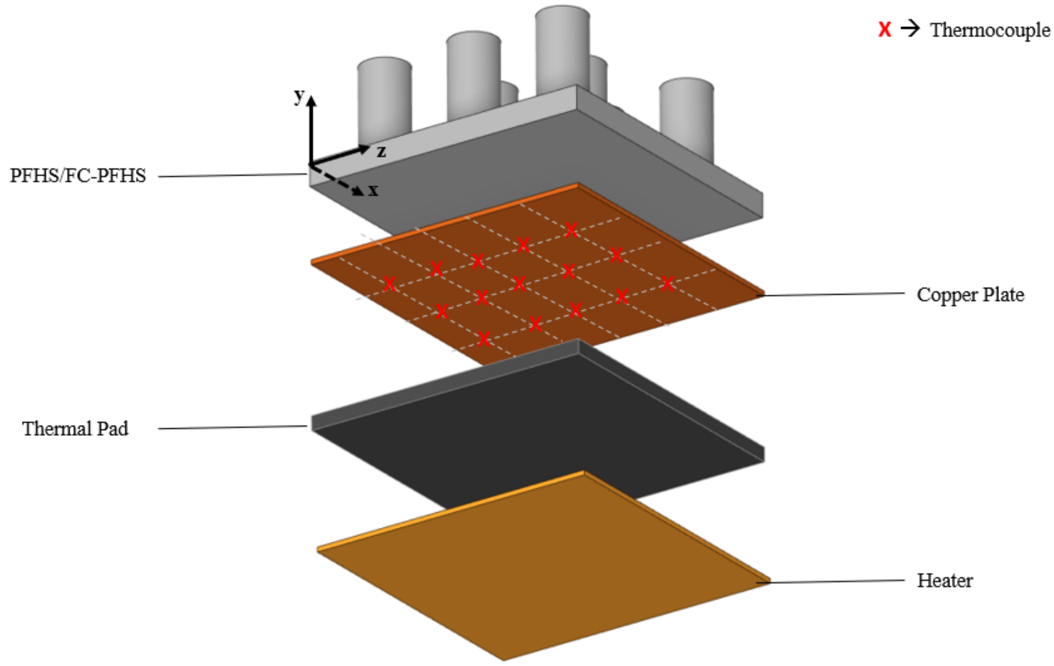

Figure 2.9 Detailed view of the bottom of the heating section

In order to adjust the power of the heater, Agilent Technologies N5771A DC power supply [53] is used (7). The velocity of the air is measured with AIRFLOW TA2 hot wire anemometer [54]. The measurement is taken from inlet channel, after the honeycombs. The pressure measurement is done by using Mesens MPS590.420 air differential pressure transmitter [55] (8) and its power is supplied by Agilent E3649A DC power supply [56] (9). The anemometer and the differential pressure transmitter are depicted in Figure 2.10. All temperature and pressure measurements are recorded by using a computer (10). The pressure readings and thermocouple readings are done using Agilent 34901A switch cards and Agilent 34972A [57] data acquisition device.

Figure 2.10 Anemometer and differential pressure transmitter

A differential pressure transmitter is an electrical device or pressure-measuring gauge designed to assess pressure differentials within a sealed container, like a pipe, utilizing two components. Various sensors, including those based on differential capacitance, vibrating wire, or strain gauges, are employed to generate an electrical signal. This signal is then transmitted to the electronics housing, where it undergoes processing, and resulting in a current or voltage output that can be interpreted by the control system and can be converted into pressure difference value [58]. The pressure measurements are taken from the inlet and exit channels for each Re as defined in Eqn. (2.2).

$$Re_{Dh} = \frac{\rho U_i D_h}{\mu} \tag{2.2}$$

where ρ and μ are fluid density and dynamic viscosity of the fluid which is air for this study. The values of the density and the dynamic viscosity of the air used are 1.164 kg/m^3 and 1.869×10^{-5} kg/m.s respectively. U_i is the inlet air velocity. The hydraulic diameter (D_h) is calculated as 0.03 m from Eqn. (2.3) with dimensions of W and H are given in Figure 2.1.

$$D_h = \frac{2 \times H \times W}{(H+W)} \tag{2.3}$$

2.1.5 Experimental Procedure

Experiments have been conducted to measure pressure drop values and to obtain heat transfer characteristics of three different heat sinks. The experiments are carried out at four Re values based on hydraulic diameter (Re_{Dh}) while maintaining a constant heat flux. The experiment matrix is provided in Table 2.4.

Table 2.4 The experiment matrix

Experiment Number	Heat Sink Type	PPI	Re_{Dh}
1	PFHS	-	1121
2	PFHS	-	1495
3	PFHS	-	1868
4	PFHS	-	2242
5	FC-PFHS	20	1121
6	FC-PFHS	20	1495
7	FC-PFHS	20	1868
8	FC-PFHS	20	2242
9	FC-PFHS	40	1121
10	FC-PFHS	40	1495
11	FC-PFHS	40	1868
12	FC-PFHS	40	2242

The experiments are conducted as follows.

i. Firstly, the inlet and outlet sections are carefully fixed to the experimental setup by screws. For all the experiments the inlet and outlet sections remained fixed while modifications are only applied to the test section.
ii. The film heater and beneath it the isolation material are placed on the bottom of the test section.
iii. On top of the film heater the test piece is carefully placed.
iv. After placing the test piece, the plexiglass channel is put on top of the test piece. The plexiglass is screwed to the experiment setup's base and also silicone is applied to it in order to ensure the air tightness.
v. Before starting the experiment, an assessment of heat loss from the test section to the environment is conducted. The power supply of the heater is

set to different values and the temperature readings from the bottom of the test piece and from the ambient are recorded. Then the heat loss for each power is determined. This operation is done only once in every test piece change.

vi. The power supply is set to 4000 W/m^2. In order to decide this value, the temperature of the heat sink is measured with different power values when the fan is at its lowest velocity value for the experiment. 4000 W/m^2 is the safest value for the heat sink not to reach 150°C which is the maximum allowable temperature for the components in the experiment work safely.

vii. The working frequency of the fan is set by the inverter.

viii. After starting the fan, the velocity of the air is measured at the entrance channel and the inverter is arranged accordingly until the desired velocity for the fan is reached.

ix. The pressure difference for the inlet and outlet section is measured by the pressure transmitter. One pipe is placed at the end of the inlet section and the other pipe is placed at the inlet of outlet section and these two pipes are connected to the pressure transmitter.

x. At each air velocity, the pressure drop measurements and the temperature of the bottom of the heatsink and the environment are recorded until the temperature change in 15 minutes would not be more than 0.2°C which is an accepted value for reaching steady state condition [59].

xi. When the experiments are over for one test piece, starting from item 3, the whole procedure is repeated in the same order.

2.1.6 Investigation of Heat Dissipation to Environment

The heat flux supplied to the film heater is calculated by multiplying the current (I) and voltage (V) value from the power supply and dividing it to the base area of the heater. For the heat dissipation to environment from the heater an experimental method which is suggested by Bogojevic et al. [60] and by Alam et al. [61] is used.

In order to calculate the heat dissipated to the environment (the remaining part of the heat supplied by the heater and not transferred to flowing air), a series of experiments is conducted.

The power supply is set to different values and the fan is turned off. For each power value, the temperature measurements for the environment (T_∞) and the bottom of the heat sink (T_{base}) are recorded until steady state conditions are reached.

When the steady state condition is reached, average temperature values for these two temperatures and their difference are calculated.

After calculating the differences in temperature, it is possible to fit a linear curve to the temperature difference and power supplied.

Then the heat dissipated to the environment (q''_{env}) can be expressed as a function of temperature difference as provided in Figure 2.11 and Eqn.s (2.4), (2.5) and (2.6).

After calculating the heat dissipated to the environment, then the net heat supplied to the flowing air can be calculated as in Eqn. (2.7).

For PFHS:

$$q''_{env} = 28.25(T_{base} - T_\infty) \tag{2.4}$$

For 20 PPI FC-PFHS:

$$q''_{env} = 27.32(T_{base} - T_\infty) \tag{2.5}$$

For 40 PPI FC-PFHS:

$$q''_{env} = 26.64(T_{base} - T_\infty) \tag{2.6}$$

And the net heat flux:

$$q''_{net} = q''_{supp} - q''_{env} \tag{2.7}$$

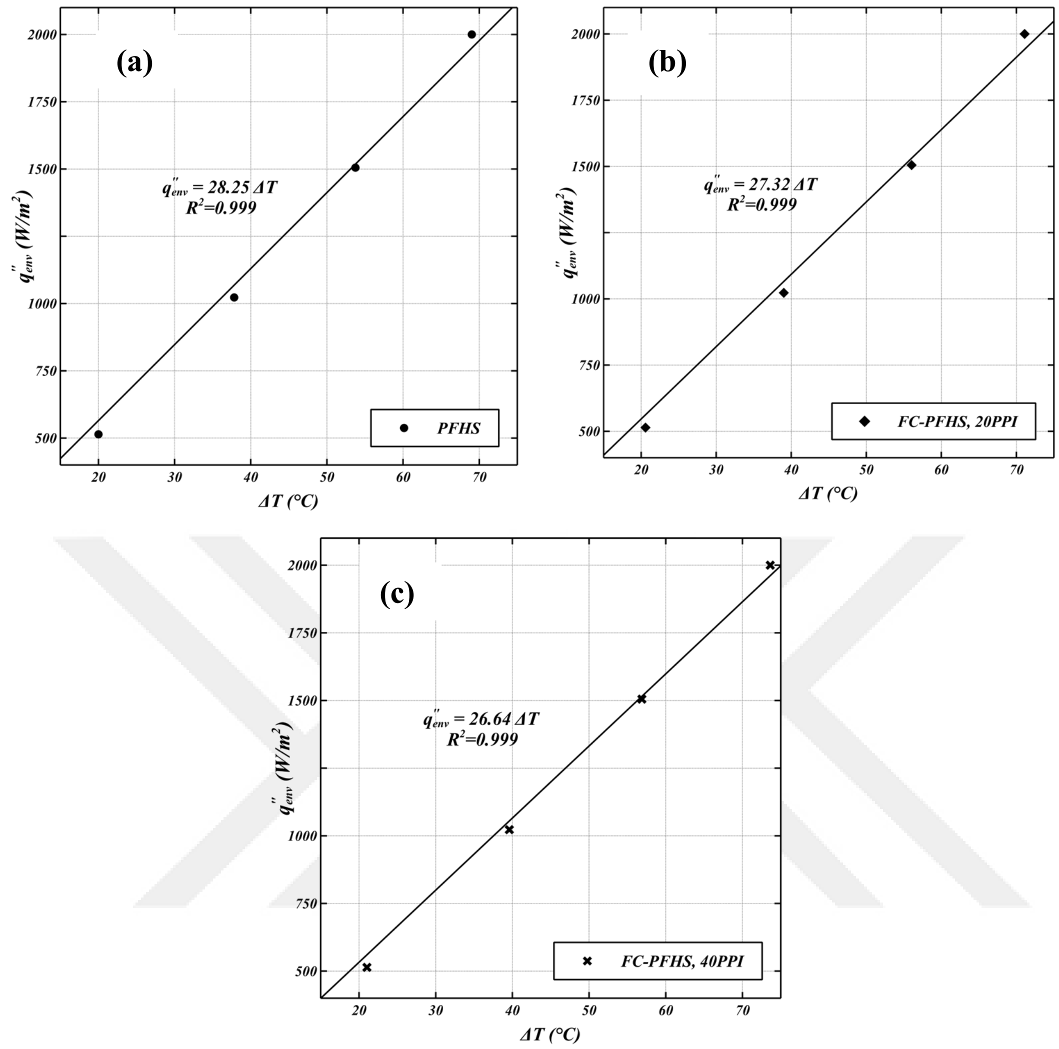

Figure 2.11 The heat dissipation for (a) PFHS, (b) 20 PPI FC-PFHS and (c) 40 PPI FC-PFHS

2.1.7 Performance Metrics

Nu is a dimensionless parameter which is used for the thermal performance evaluation of the FC-PFHSs. Nu can be calculated as,

$$Nu = \frac{(q''_{supp} - q''_{env})D_h}{(T_{base} - T_i)k_f} \tag{2.8}$$

where q''_{supp} is the heat flux supplied to the heat sink. q''_{env} is heat flux dissipated to the environment. T_{base} is the average base temperature of the heat sink, T_i is the inlet air temperature and k_f is thermal conductivity of air.

Performance evaluation criterion (PEC) represents the influence of the attempt on heat transfer enhancement with the pressure drop compared to a reference configuration [62]. This parameter is used commonly in literature for evaluating the heat transfer enhancement compared to the pressure drop [38,63,64]. It can be defined as follows:

$$PEC = \frac{Nu/Nu_0}{\left(\frac{\Delta P}{\Delta P_0}\right)^{1/3}} \tag{2.9}$$

where Nu_0 and ΔP_0 stands for the Nu and pressure drop for the base case which the performance will be compared.

2.1.8 Uncertainty Analysis

Uncertainty values of the quantities measured in the experimental study are calculated using the Gauss error propagation law given in Eqn. (2.10) [65].

$$w_R = \sqrt{\left(\frac{\partial R}{\partial x_1} w_1\right)^2 + \left(\frac{\partial R}{\partial x_2} w_2\right)^2 + \cdots + \left(\frac{\partial R}{\partial x_n} w_n\right)^2} \tag{2.10}$$

In this formula, R is the measured value as a function of x_1, x_2, … x_n and w_n is the uncertainty value of the n_{th} measured value. The uncertainty value of the measurement devices are the catalog values provided for each device.

Table 2.5 Uncertainty values of the measuring devices

Measuring device	Uncertainty
T-type thermocouple [66]	±1°C
Anemometer [54]	±0.05 m/s
Pressure transmitter [55]	±0.5%

Then the maximum uncertainty values for Re and Nu for the experiment are calculated as 8% and 5.8%, respectively. Despite the potential fluctuations or uncertainties, this value is not as high as to have a significant impact on the behavior of the flow, particularly due to the low velocities observed in the experimental conditions. Thus, it can be deemed acceptable.

2.2 Numerical Study

A numerical model is created in order to further analyze the hydrothermal characteristics of FC-PFHSs. The model is firstly validated with the experimental results and after validation parameters affecting the heat transfer and pressure drop characteristics of FC-PFHSs have been investigated. The porosity of the metal foam and the geometry of the heat sink are among these parameters. Due to constraints in both time and cost, it is not feasible to experimentally investigate the effects of these parameters. Therefore, within the scope of this thesis, the effects of these parameters are studied with the validated numerical model.

2.2.1 Computational Domain

The geometry of the aluminum foam is too complicated to be implemented in the computational domain. Therefore, the conjugate heat transfer model is not utilized. Instead, porous domain is defined for the cladded aluminum foams. At the end of the simulations, in order to validate the numerical model, the results of the simulations are compared with the experimental ones in terms of T_{base} and ΔP.

Since there is symmetricity with respect to z=W/2 plane, half of the heat sinks are modeled as computational domain. Also, the inlet and outlet channels are not included in the domain. The hydrodynamic entry length ($x_{fd,h}$) for a fully developed flow corresponds to the length in an internal flow after which the viscous effects extend over and the velocity profile no longer changes [67]. It can be evaluated for laminar flows as:

$$x_{fd,h} = 0.05 * Re_{Dh} * D_h \tag{2.11}$$

For the highest Re considered in this thesis, the value is obtained around 3 m, which is significantly larger than the channel length in the experiment setup. For the cooling of electronic components such a length is not feasible. Therefore, in the experiments, the channel length is constrained to a reasonable value and the inlet and outlet channels are not included in the numerical study. The computational domain is provided in Figure 2.12.

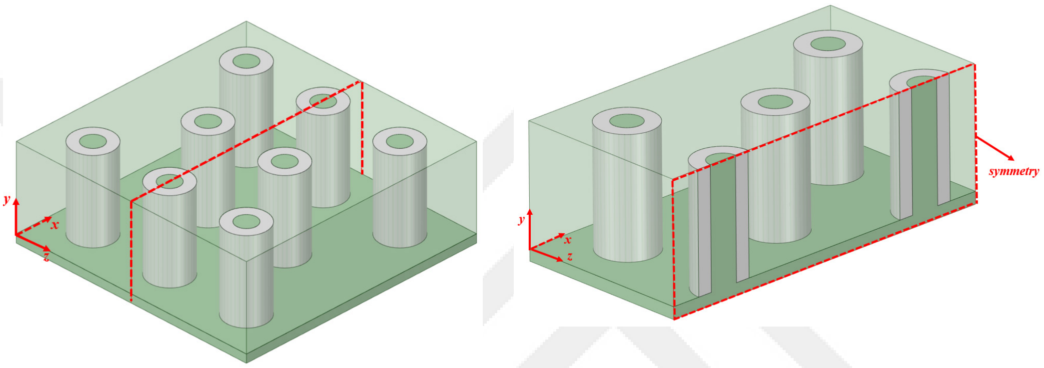

Figure 2.12 Computational domain with and without symmetry

2.2.2 Governing Equations and Boundary Conditions

The assumptions used in numerical model are:

- The air is Newtonian, laminar, steady, and incompressible.
- Local thermal equilibrium (LTE) between the foam and the air is assumed, since the temperature gradient between the fluid and solid structure are low and the porous foams have very narrow bonds [36].
- Viscous dissipation, natural convection and radiative heat transfer are neglected.
- Changes in thermo-physical properties of the fluid and solid phases with temperature are neglected.

The governing equations for air domain are given as follows:

Continuity Equation:

$$\nabla.\vec{\boldsymbol{U}}_{\boldsymbol{air}} = 0 \tag{2.12}$$

Momentum Equation:

$$\rho_{air}(\vec{\boldsymbol{U}}_{\boldsymbol{air}}.\nabla)\vec{\boldsymbol{U}}_{\boldsymbol{air}} = -\nabla P_{air} + \mu_{air}\nabla^2\vec{\boldsymbol{U}}_{\boldsymbol{air}} \tag{2.13}$$

Energy Equation:

$$\rho_{air}c_{pair}\vec{\boldsymbol{U}}_{\boldsymbol{air}}.\nabla T_{air} = \nabla.[(k_{air})\nabla T_{air}] \tag{2.14}$$

The governing equations for porous domain, which includes both the aluminum foam and the air inside its pores, are given as follows:

Continuity Equation:

$$\nabla.\vec{\boldsymbol{U}}_{\boldsymbol{p}} = 0 \tag{2.15}$$

With the assumptions mentioned to describe the fluid flow for porous zone Forchheimer-Brinkman extended Darcy model is used.

Momentum Equation:

$$\frac{\rho_p}{\varepsilon^2}\left(\vec{\boldsymbol{U}}_{\boldsymbol{p}}.\nabla\right)\vec{\boldsymbol{U}}_{\boldsymbol{p}} = -\nabla P_p + \frac{\mu_p}{\varepsilon}\nabla^2\vec{\boldsymbol{U}}_{\boldsymbol{p}} - \left(\frac{\mu_p}{K} + \frac{\rho_p c_F}{\sqrt{K}}\left|\vec{\boldsymbol{U}}_{\boldsymbol{p}}\right|\right)\vec{\boldsymbol{U}}_{\boldsymbol{p}} \tag{2.16}$$

And assuming LTE between the porous region and the fluid the conservation of energy equation becomes:

$$(\rho_p c_{p,p})\vec{\boldsymbol{U}}_{\boldsymbol{p}}.\nabla T_p = k_{eff}\nabla^2 T_p \tag{2.17}$$

The conduction equation for solid media:

$$k_{Al}\nabla^2 T_{Al} = 0 \tag{2.18}$$

k_{eff} is the effective thermal conductivity which can be calculated as [38]:

$$k_{eff} = \varepsilon k_{air} + (1-\varepsilon)k_{Al} \tag{2.19}$$

U is the velocity magnitude, ρ is the density, P is the pressure, μ is the dynamic viscosity, c_p is the specific heat, T is the temperature, k is the thermal conductivity, ε is the porosity, C_F and K are inertial coefficient and permeability respectively.

The subscript p indicates porous domain and Al indicates aluminum domain.

The schematic view of the coordinate system and boundaries can be depicted in Figure 2.13.

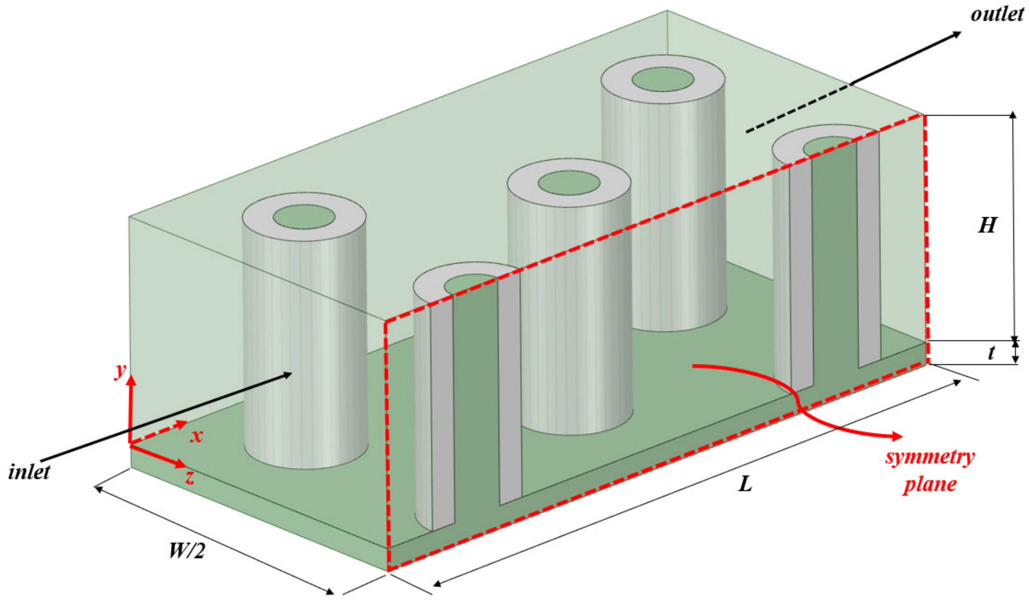

Figure 2.13 Schematic view of the computational domain and boundaries

To study the physical characteristics of heat transfer and fluid flow within pin fins, a variety of boundary conditions including inlet, outlet, wall, and symmetry are applied within the computational domain.

The boundary conditions used in the numerical simulations are provided in Table 2.6.

Table 2.6 Boundary conditions

Boundary (x,y,z)	**Condition**
Inlet (x=0, -t≤y≤0, z)	Insulated
Inlet (x=0, 0≤y≤H, z)	Flow inlet, T=Ti (°C), U=U_i (m/s)
Right (x, -t≤y≤H, z=W/2)	Symmetry
Left (x, y, z=0)	No-slip and insulated
Top (x, y=H, z)	No-slip and insulated
Bottom (x, y=0, z)	No-slip
Bottom (x, y=-t, z)	Constant heat flux, q″ (W/m^2)
Outlet (x=L, -t≤y≤0, z)	Insulated
Outlet (x=L, 0≤y≤H, z)	P_{gauge}=0 Pa

It is important to note that at the beginning of the iterative numerical solution, a hybrid initialization method is used to estimate the velocity and pressure fields [68] using the Euler equation. The initial temperature is assumed to be 20 °C at the first iteration.

The governing equations with relevant boundary conditions are discretized using the finite volume method (FVM) with a second-order upwind scheme applied to pressure, momentum, and energy equations. A Coupled scheme is employed to solve these equations, incorporating a pseudo-transient time-stepping approach for improved convergence. The convergence criteria for the residuals of all variables except energy are chosen to be 10^{-6} and for energy, the criterion of 10^{-9} is set. The geometry creation, meshing and solving of the governing equations are done by using ANSYS SpaceClaim, ANSYS Meshing, and ANSYS FLUENT 2023 R1.

2.2.3 Mesh Independence Study

In order to ensure the reliability of the numerical simulations, a mesh independence study is conducted. Three different meshing configurations for the highest Re during the experiments have been studied to observe the effects of the number of the elements to the results of the temperature and pressure drop. The results are provided in Table 2.7.

Table 2.7 The results of the mesh independence study

	Elements	Nodes	T_{base} (°C)	% Change in T_{base}	ΔP (Pa)	% Change in ΔP
PFHS	1670271	959950	56.11	-	5.65	-
	3840987	1596130	56.26	0.27	5.72	1.24
	9085723	3858842	56.55	0.52	5.76	0.70
20 PPI FC-PFHS	2110702	1683635	49.7	-	5.53	-
	3508660	1974275	49.8	0.20	5.6	1.27
	8651487	3047433	49.79	0.02	5.66	1.07
40 PPI FC-PFHS	2110702	1683635	53.83	-	6.84	-
	3508660	1974275	53.88	0.10	6.89	0.78
	8651487	3047433	53.87	0.02	6.96	0.93

As evident from Table 2.7, variations in the number of elements only influence the results by a maximum of 0.52% for the base temperature and 1.27% for pressure drop.

Given the significantly low maximum variation value and considering computational costs and efforts, an element number of 3840987 for PFHS and 3508660 for FC-PFHSs is sufficient to ensure numerical accuracy in the simulations.

The meshing configurations are presented in Figure 2.14.

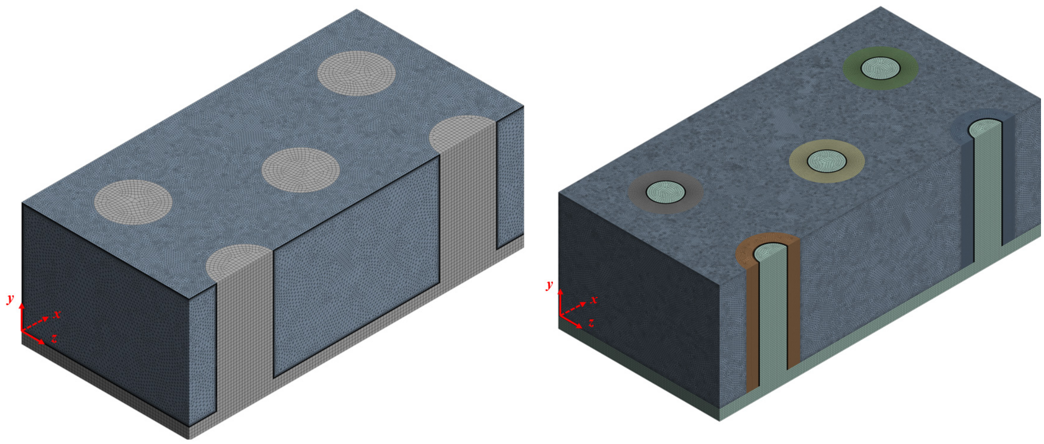

Figure 2.14 Meshing configurations for (a) PFHS, (b) 20 PPI FC-PFHS

The detailed meshing configuration on symmetry plane for FC-PFHS is given in Figure 2.15.

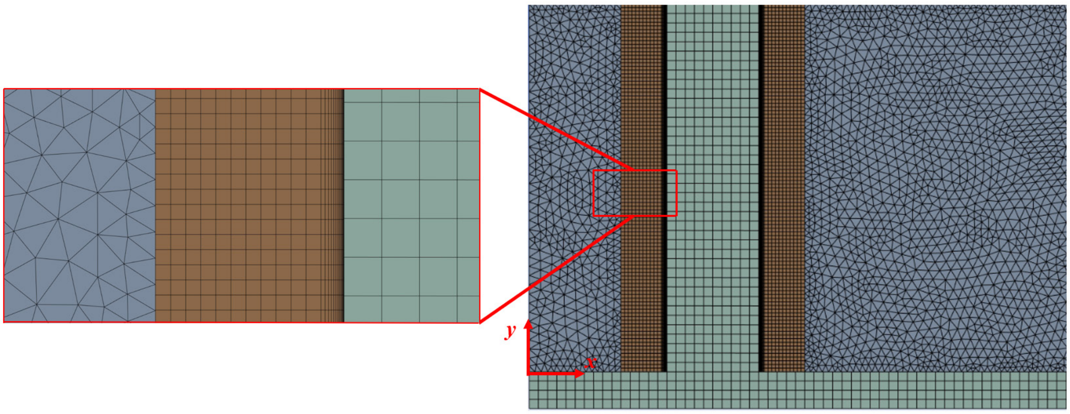

Figure 2.15 Detailed meshing configuration on symmetry plane for 20 PPI FC-PFHS

2.2.4 Parametric Study

For the scope of parametric study, the outer diameter of the cladded aluminum foam (D_{AF}) is increased while the pin fin diameter (D_{PF}) is kept constant at 5mm. Two different geometries have been created.

As a second parameter, the porosity of the aluminum foams has been changed while PPI value is kept constant at 20 PPI. With the changing porosity value, the inertial coefficient and permeability constants also change.

The porosity values are chosen from the literature which the C_F and K_F values are provided. Each scenario in parametric study is called as "Case".

The cases are studied for the lowest Re during the experiments, since it results in the maximum base temperature, which is the critical consideration for electronic components.

The list of parameters studied is provided in Table 2.8.

Table 2.8 Parametric study matrix

Case	D_{PF} (mm)	D_{AF} (mm)	ε	C_F	K_F x 10^7 (m^2)
PFHS_Base	5	-	-	-	-
FC-PFHS_Ref	5	10	0.95	0.093	1.30
FC-PFHS_Case1	5	10	0.93	0.098	1.17
FC-PFHS_Case2	5	10	0.92	0.102	1.06
FC-PFHS_Case3	5	10	0.90	0.088	0.90
FC-PFHS_Case4	5	15	0.95	0.093	1.30
FC-PFHS_Case5	5	15	0.93	0.098	1.17
FC-PFHS_Case6	5	15	0.92	0.102	1.06
FC-PFHS_Case7	5	15	0.90	0.088	0.90
FC-PFHS_Case8	5	18	0.95	0.093	1.30
FC-PFHS_Case9	5	18	0.93	0.098	1.17
FC-PFHS_Case10	5	18	0.92	0.102	1.06
FC-PFHS_Case11	5	18	0.90	0.088	0.90

FC-PFHS_Ref **(up to this point this case is called as 20 PPI FC-PFHS, from this point on it will be stated as FC-PFHS_Ref)** is studied both experimentally and numerically, while all other cases are studied only numerically. For this reason, this case is specifically named as FC-PFHS_Ref.

CHAPTER 3

RESULTS AND DISCUSSION

In this chapter, the results obtained from both experimental and numerical studies will be presented and discussed. Initially, the results of the experimental and numerical study will be provided and the numerical model will be validated. Subsequently, thermal and hydrothermal performance of heat sinks will be compared and a parametric analysis will be conducted on the heat sink exhibiting the most favorable hydrothermal performance. The focus of the parametric analysis will be to explore the influence of varying geometric configurations and the utilization of foams with different porosities on hydrothermal performance. This investigation aims to show how changes in geometry and foam characteristics impact the hydrothermal behavior of the system. After the parametric study, with the help of PEC value, the heat sink which has the best hydrothermal performance will be presented. Furthermore, an investigation into local hot spots will be conducted in order to ascertain whether there exist local hot spots on the base plate of the heat sink.

3.1 Validation of Numerical Models

3.1.1 Pin Fin Heat Sink

The comparison between the base temperature and pressure drop values obtained from both experiments and numerical simulations for the PFHS aims to verify the accuracy and reliability of the numerical model. The results obtained are provided in Figure 3.1.

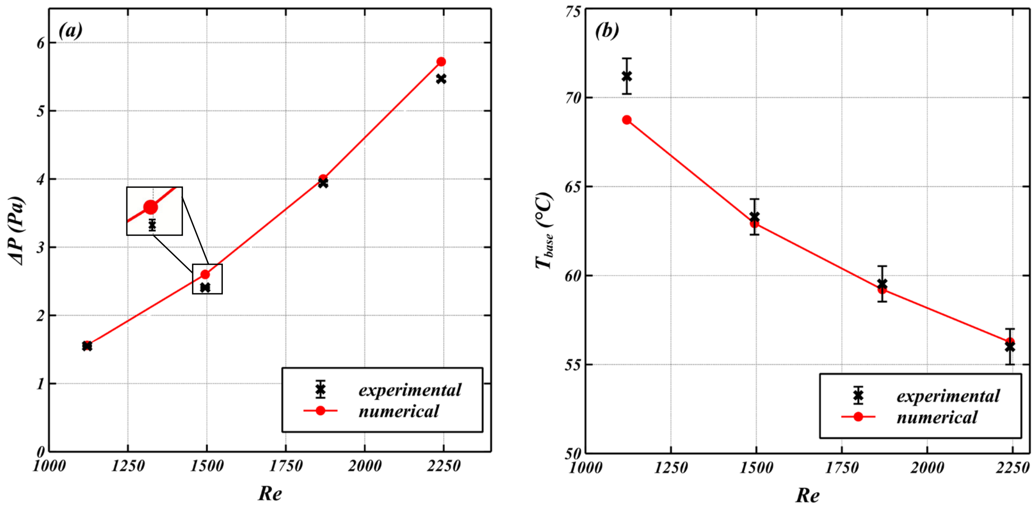

Figure 3.1 Experimental and numerical results for PFHS

The experimental and numerical results are in good agreement in terms of pressure drop and base temperature. The maximum deviation for the pressure drop is 8% while for base temperature it is 3.5%.

3.1.2 FC-PFHS_Ref and 40 PPI FC-PFHS

While cladding foam onto pin fins, it is not possible to clad it perfectly. As a result of cladding, there exist gaps between the foam and the pin fin which resulted in thermal contact resistance (TCR) between the foam and the pin fin for both FC-PFHS_Ref and 40 PPI FC-PFHS. In order to determine the TCR value, the existing literature studies have been investigated. Jaeger et al. [69] has conducted an experimental study for the investigation of TCR for four bonding methods. The authors figured out that TCR for epoxy bonding applied under 0.5 MPa pressure is 0.00125 m^2K/W. But in this study, the epoxy bonding is applied without any external pressure. Therefore, the TCR value between the foam and pin fins is taken to be 0.003 m^2K/W in numerical modelling. The comparison of the experimental and the numerical simulation results for FC-PFHS_Ref and 40 PPI FC-PFHS are depicted in Figure 3.2.

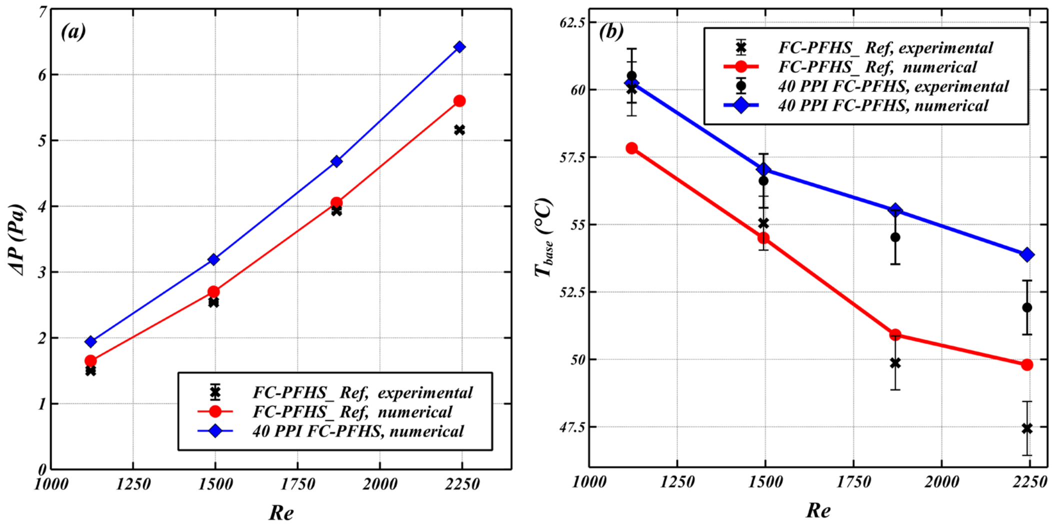

Figure 3.2 Experimental and numerical results for FC-PFHS_Ref and 40 PPI FC-PFHS

For FC-PFHS_Ref the maximum variation between the experiments and numerical study obtained for the pressure drop is 10%. Considering the low pressure drop value, this variation is acceptable.

On the other hand, for FC-PFHS_Ref the maximum variation is 4.2% for the base temperature. When the Re increases the behavior of the experimental and numerical results tend to vary. At high Re, numerical calculations estimate higher base temperature than the experiment while this behavior is opposite for low Re.

For 40 PPI FC-PFHS, the pressure transmitter used in the experiments failed in measuring the pressures for each Re, since pressure drop values are quite low. Therefore, pressure drop measurements couldn't be included in the validation of the 40 PPI FC-PFHS. For the temperature, the maximum variation between experimental and numerical study is found to be only 3.7%.

The numerical model is in good agreement with the experiments considering the maximum variation values. Therefore, it can be stated that the numerical model has been successfully validated and can be utilized for further considerations.

3.1.3 Flow Regime

During numerical modelling, the flow is taken to be a laminar flow. In order to make sure that the flow is laminar throughout the channel for Re used in parametric study, the flow regime over a pin fin is investigated. The Re values calculated based on a single pin fin or hydraulic diameter of the channel are always below 2300, so the laminar flow assumption is valid.

The velocity contours for fluid and porous domain and the temperature contour for fluid, solid and porous domains when Re_{Dh}=2242 are given in Figure 3.3. The velocity contour is taken on xz plane at y=H/2, while the temperature contour is taken on xy plane on symmetry axis (z=W/2). From the velocity profile it can be observed that laminar flow consideration is valid since at the entrance the streamlines are relatively straight and parallel, aligning with the flow direction imposed by the channel walls. Some initial distortion of streamlines occurs near foam's surface due to the interaction between the air and the foam. Streamlines closer to the aluminum foam and pin fin curve more sharply due to the influence of the FC-PFHS surface. It can be clearly depicted that streamlines attach to the surface of the pin fin as the air flows around it which is due to the no-slip condition. After passing the pin fins, the streamlines gradually separate and straighten out as the flow re-establishes itself.

The velocity profile for both of the FC-PFHS is quite similar while temperature profile differs from each other. From the temperature contour on the symmetry axis, it can be observed that the thermal boundary layer above the FC-PFHS_Ref is thinner than 40 PPI FC-PFHS. Considering the lower base temperature values obtained for FC-PFHS_Ref, this is an expected scenario. Also, the maximum temperature on the temperature contour on FC-PFHS_Ref is lower than the 40 PPI FC-PFHS.

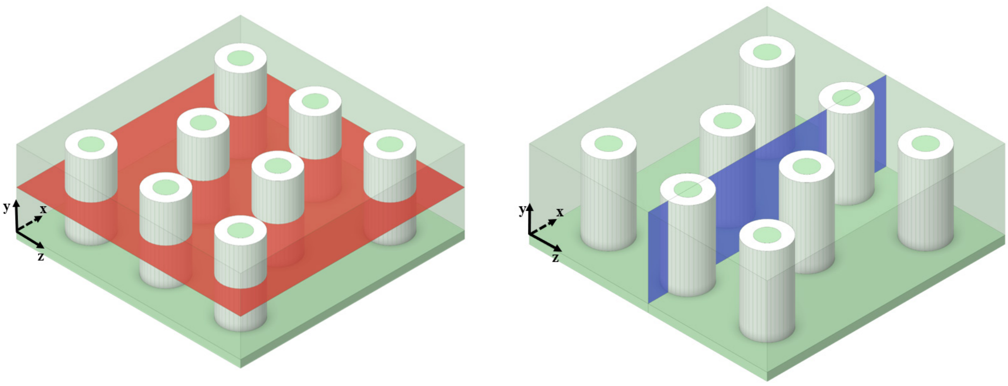
y
x
z
y
x
z

(a)

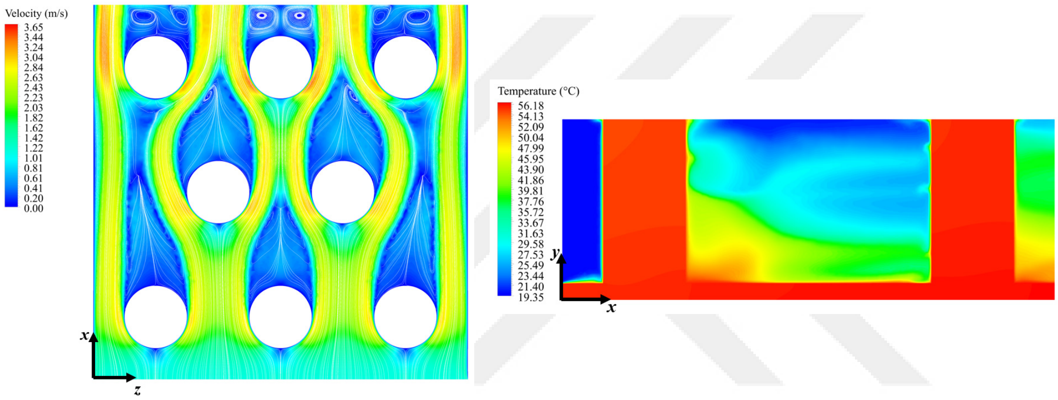
Velocity (m/s)
3.65
3.44
3.24
3.04
2.84
2.63
2.43
2.23
2.03
1.82
1.62
1.42
1.22
1.01
0.81
0.61
0.41
0.20
0.00
x
z
Temperature (°C)
56.18
54.13
52.09
50.04
47.99
45.95
43.90
41.86
39.81
37.76
35.72
33.67
31.63
29.58
27.53
25.49
23.44
21.40
19.35
y
x

(b)

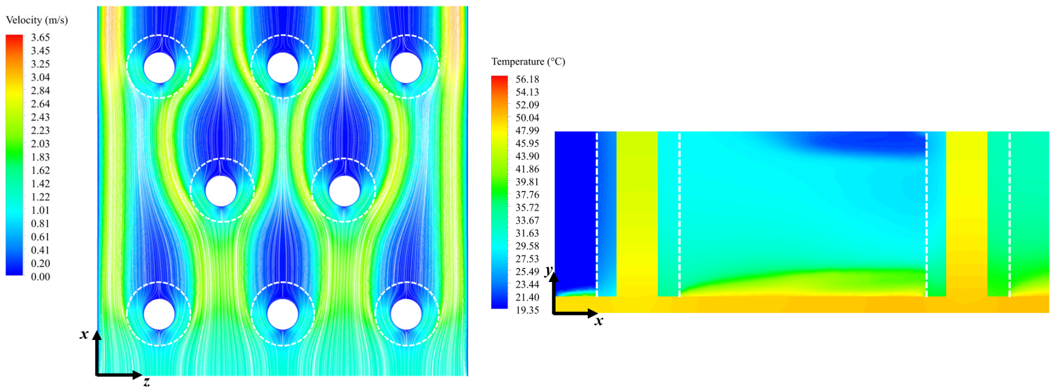
Velocity (m/s)
3.65
3.45
3.25
3.04
2.84
2.64
2.43
2.23
2.03
1.83
1.62
1.42
1.22
1.01
0.81
0.61
0.41
0.20
0.00
x
z
Temperature (°C)
56.18
54.13
52.09
50.04
47.99
45.95
43.90
41.86
39.81
37.76
35.72
33.67
31.63
29.58
27.53
25.49
23.44
21.40
19.35
y
x

(c)

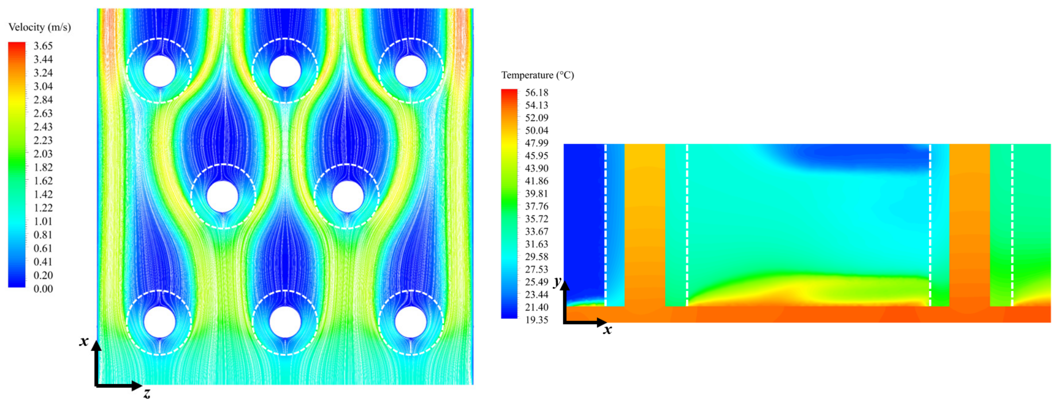

Figure 3.3 The velocity and temperature contours for (a) PFHS with D_{PF}=10mm (b) FC-PFHS_Ref, (c) 40PPI FC-PFHS

3.2 Comparison of PFHS and FC-PFHSs with Different PPI Values

With the validated numerical model, the thermal performances of PFHS, FC-PFHS_Ref and 40 PPI are investigated. As provided in Figure 3.4 for all Re, FC-PFHS_Ref demonstrates superior thermal performance, showing a Nu increase of approximately 20% compared to 40 PPI FC-PFHS and 37.5% relative to PFHS.

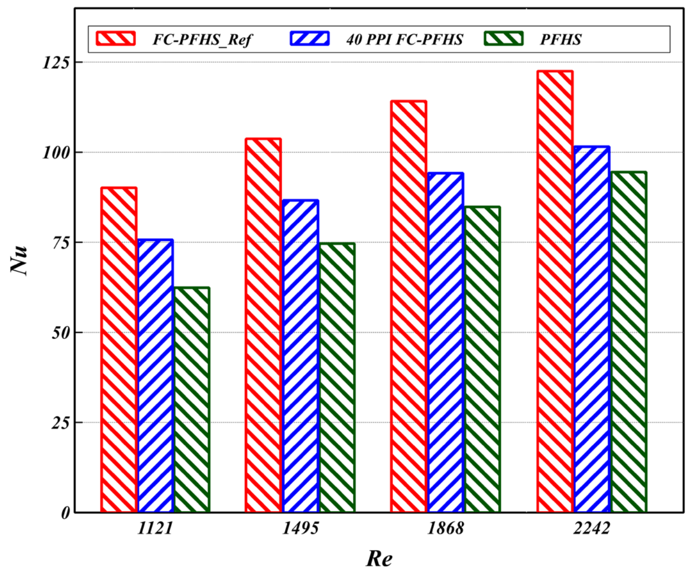

Figure 3.4 Nu for FC-PFHS_Ref, 40 PPI FC-PFHS and PFHS

And the hydrothermal performance of FC-PFHS_Ref and 40 PPI FC-PFHS are compared by using PEC value. For the evaluation of PEC value, the base case which the performance comparison made is taken to be the PFHS for each Re. In Figure 3.5, PEC value variation of FC-PFHS_Ref and 40 PPI FC-PFHS is provided. Since pressure couldn't be measured during the experiment of 40 PPI FC-PFHS, PEC value is calculated by only using the results from numerical study.

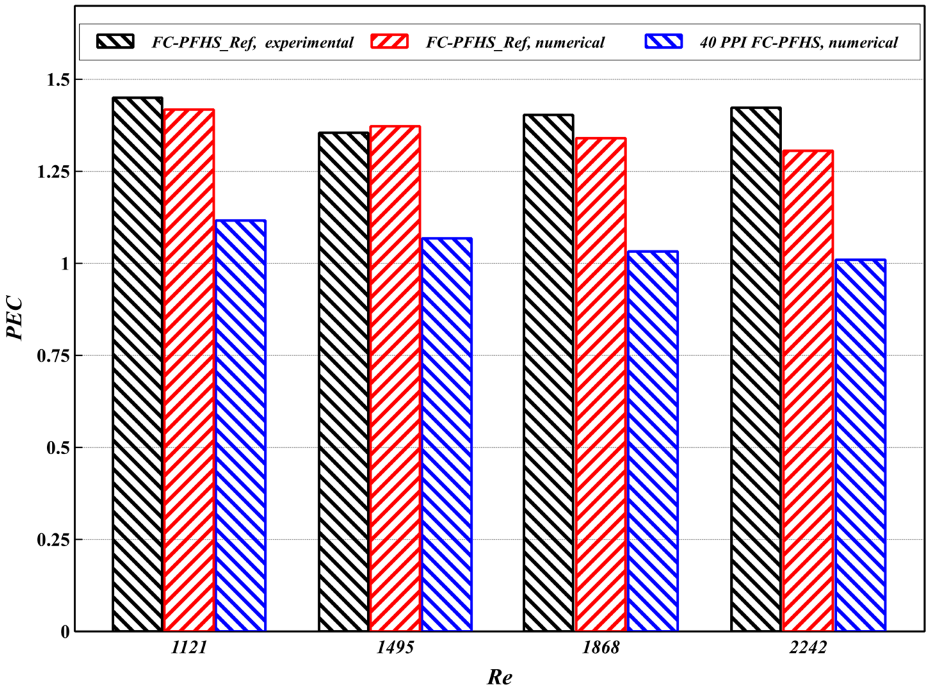

Figure 3.5 PEC of FC-PFHS_Ref and 40 PPI FC-PFHS

It can be observed that PEC of FC-PFHS_Ref is higher in both experimental and numerical cases compared to the 40 PPI FC-PFHS. Consequently, in the context of hydrothermal performance, FC-PFHS_Ref demonstrates superior performance relative to the 40 PPI FC-PFHS. All in all, cladding aluminum foam onto the pin fin can potentially enhance hydrothermal performance by up to 45% compared to the PFHS alone.

3.3 Parametric Study Results

Based on the experimentally validated numerical model, it is observed that the hydrothermal performance of FC-PFHS_Ref is superior to 40 PPI FC-PFHS. Hence, the parametric study is specifically focused on the 20 PPI FC-PFHS for all the cases defined in Table 2.8. Also, the numerical model is validated for both base temperature and pressure drop for 20 PPI FC-PFHS, which makes the parametric study justified for this FC-PFHS.

Figure 3.6 depicts the parametric study results for 0.95, 0.93, 0,92 and 0.90 porosity values. All of the figures include PFHS_Base in order to visualize the hydrothermal performance enhancement.

When the thickness of the cladding increases for the same porosity value Nu increases due to the enlarged heat transfer area. However, simultaneously, the pressure drop value also increases with the foam thickness increment.

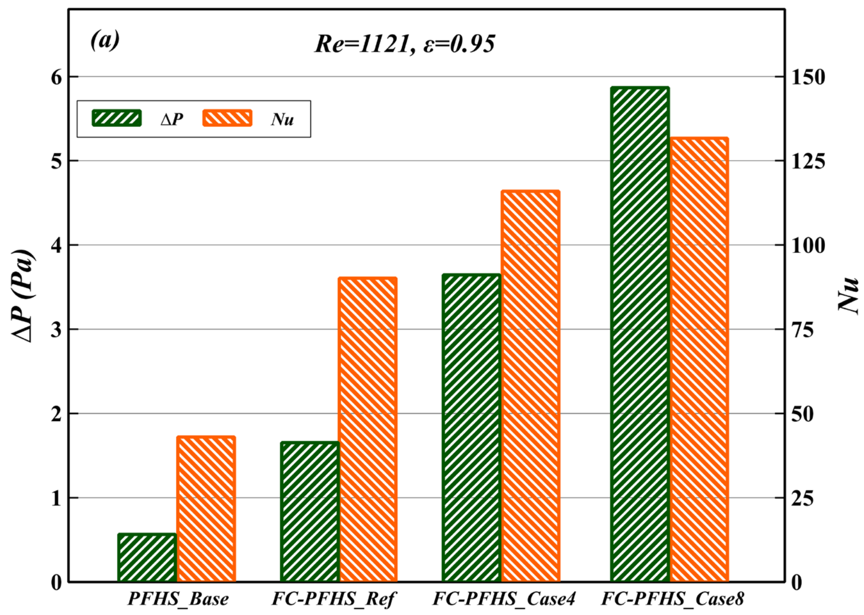

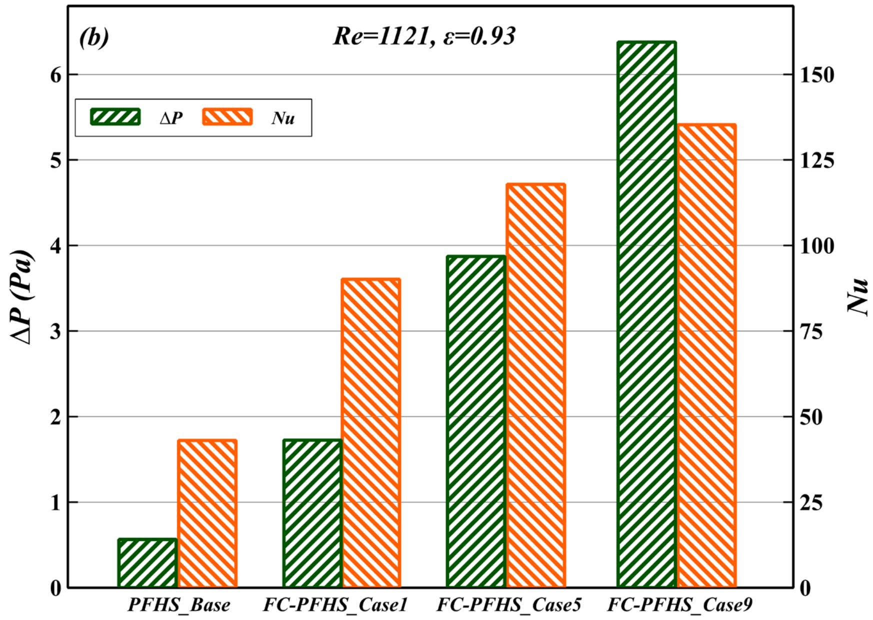
(b)
Re=1121, ε=0.93
ΔP
Nu
ΔP (Pa)
Nu
0
1
2
3
4
5
6
0
25
50
75
100
125
150
PFHS_Base
FC-PFHS_Case1
FC-PFHS_Case5
FC-PFHS_Case9

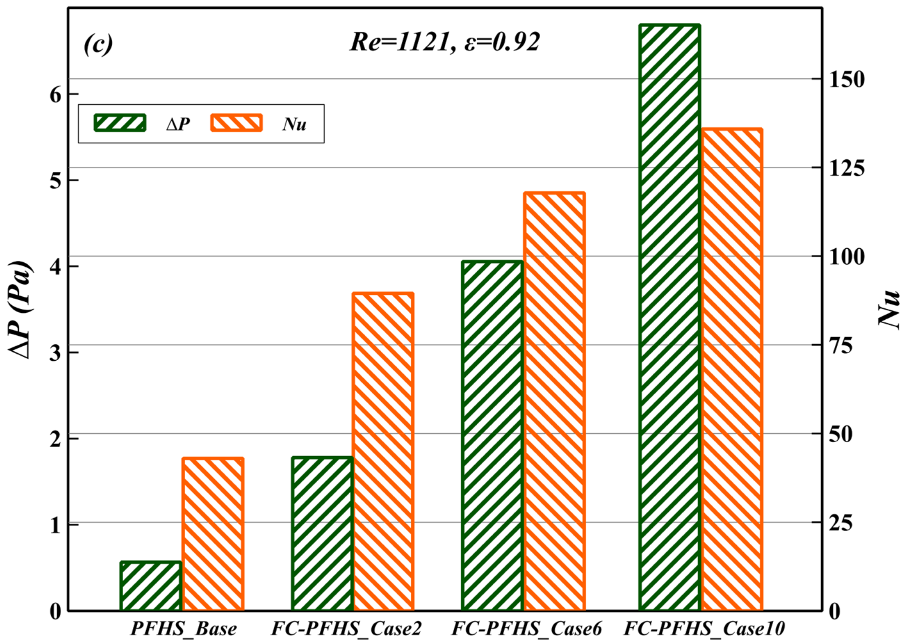
(c)
Re=1121, ε=0.92
ΔP
Nu
ΔP (Pa)
Nu
0
1
2
3
4
5
6
0
25
50
75
100
125
150
PFHS_Base
FC-PFHS_Case2
FC-PFHS_Case6
FC-PFHS_Case10

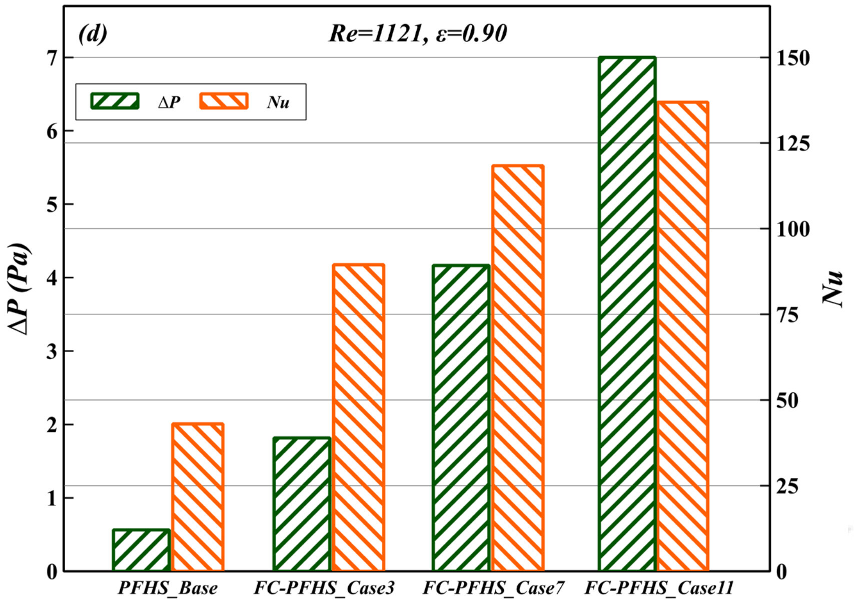

Figure 3.6 ΔP and Nu of parametric study cases

For the cases with same cladding thickness but different porosity value, when porosity decreases, the pressure drop increases. While the porosity decreases, the permeability value decreases which results in higher pressure drop. Thus, for applications with low pumping power requirements, foams with higher porosity may be preferred.

The variation of porosity value does not affect the Nu for the same cladding thickness. Changes in porosity lead to corresponding alterations in other parameters such as permeability, coefficient of inertia and k_{eff}, which are sourced from existing literature. Consequently, changes in porosity lead to variations in parameters which are obtained experimentally and at the end, it is not possible to determine the effect of porosity on thermal performance within studied Re values. For a different study which has higher Re than current study, it may be possible to observe the effect of change in porosity on heat transfer performance.

For all of the cases it can be clearly stated that there is a significant improvement in the thermal performance of the cases studied compared to the base case. For the hydrothermal performance, PEC value will be utilized in the upcoming sections.

In order to observe the effect of foam cladding thickness on hydrothermal performance deeply, the velocity and temperature profiles of three cases have been investigated. All of the cases have the same porosity value, which the experiments are conducted.

In Figure 3.7 the velocity contour is taken on xz plane at y=H/2 and the temperature contour is taken on symmetry plane. The dashed lines in the figures present the outer boundary of the cladded foam.

As the thickness of the aluminum foam increases, the heat transfer area expands, leading to a decrease in the maximum temperature observed across the entire domain.

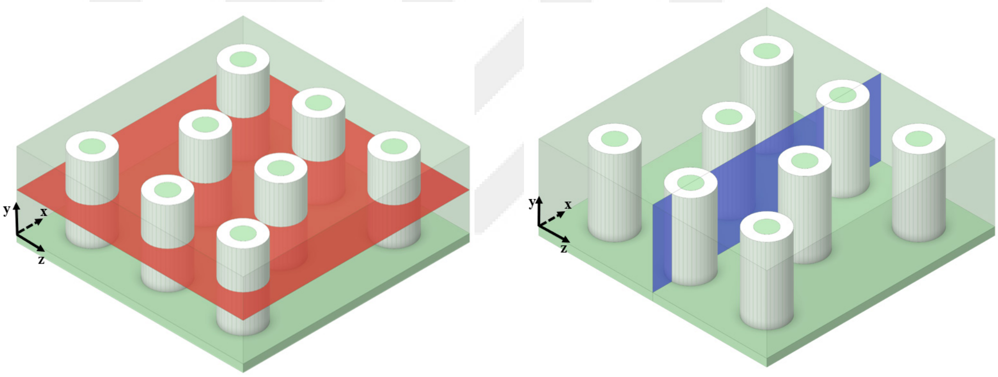

(a)

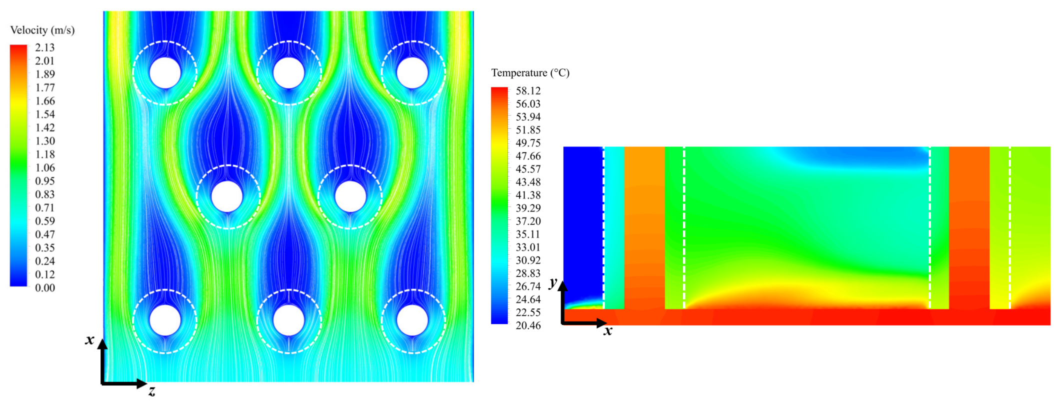

(b)

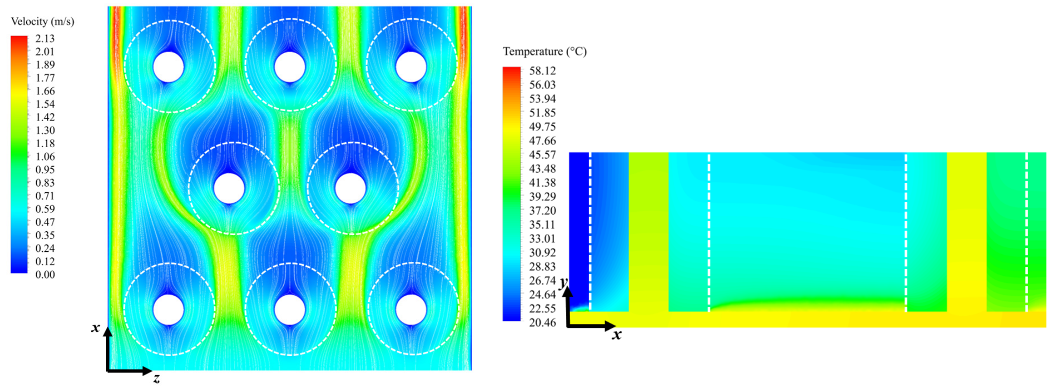

(c)

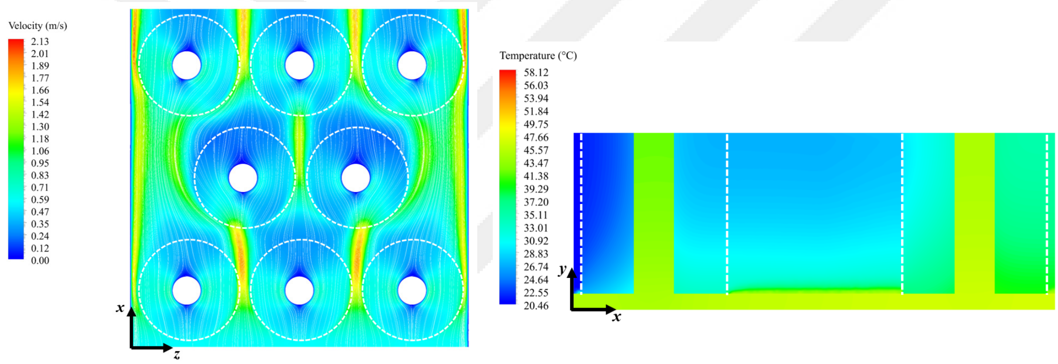

Figure 3.7 Velocity and temperature profile for (a) FC-PFHS_Ref, (b) FC-PFHS_Case4, (c) FC-PFHS_Case8

Also, it can be observed that the thickness of the thermal boundary layer decreases while the cladding thickness increases. A thinner thermal boundary layer comes with the advantage of higher flow mixing capacity and therefore higher Nu. However, the enhancement in thermal performance is accompanied by the drawback of an increased pressure drop, resulting in higher power consumption.

For the overall hydrothermal performance, PEC for all of the cases has been calculated and provided in Figure 3.8. For all different pin fin diameter cases, the first, second, third and fourth bars represent cases with 0.95, 0.93, 0.92 and 0.90 porosity, respectively. Among these cases, FC-PFHS_Ref demonstrates the most favorable hydrothermal performance, showcasing a notable enhancement of 46.45%. It is noteworthy that all studied scenarios exhibit considerable improvements in hydrothermal performance, even the case with the lowest enhancement, FC-PFHS_Case11, which still achieves an improvement of 37.5%. Consequently, cladding foams onto pin fins exhibits improved heat transfer capabilities despite a noticeable increase in pressure drop.

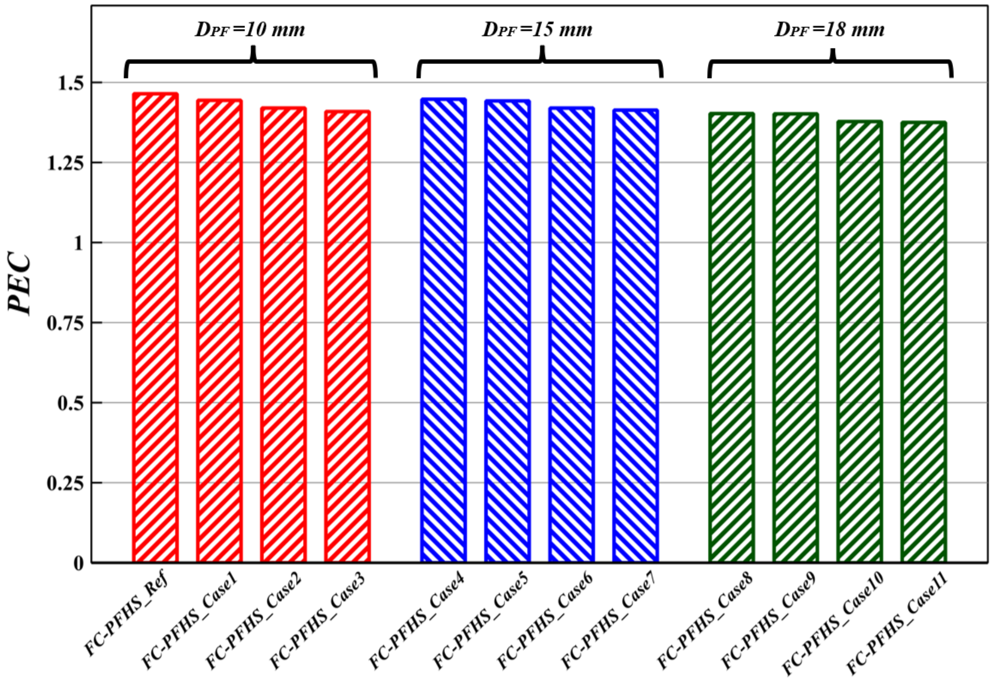

Figure 3.8 PEC values for the parametric study

3.3.1 Local Hot Spot Investigation

During the cooling process of electronic components, the distribution of temperatures across the component may vary, resulting in the occurrence of localized regions experiencing higher temperatures compared to adjacent areas. This phenomenon is commonly referred to as local hot spots, where specific zones within the electronic device exhibit elevated thermal levels.

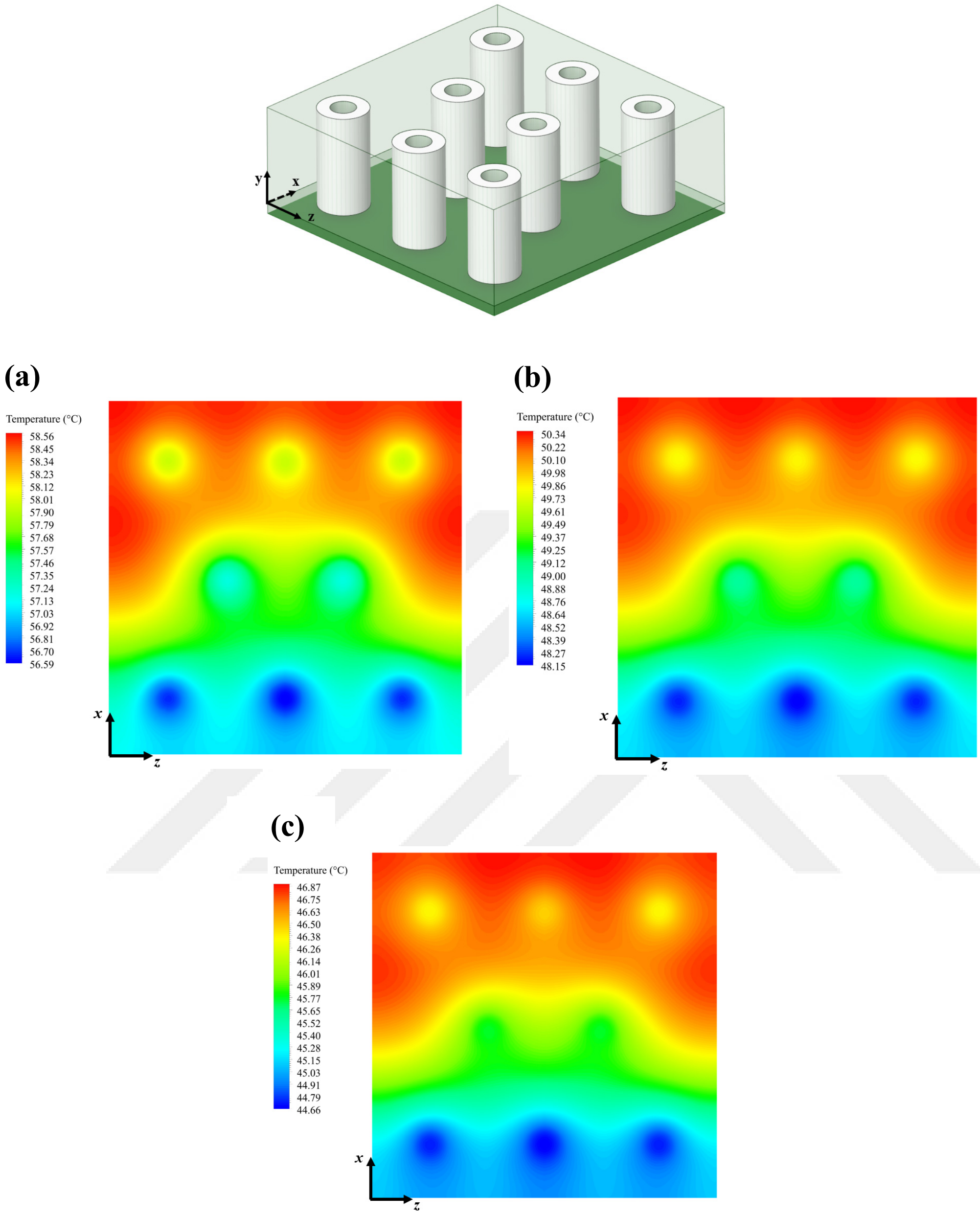

Figure 3.9 Local temperature distribution of base plate for (a) FC-PFHS_Ref, (b) FC-PFHS_Case4 and (c) FC-PFHS_Case8

Ensuring effective cooling is essential for the proper functioning of electronic components, necessitating a cooling system capable of mitigating local hot spots. Therefore, in addition to examining the hydrothermal performance of cases within the parametric study, it is crucial to analyze the behavior of local hotspot generation to ensure the system operates safely and reliably.

The temperature distribution on the base plate (xz plane when y=-t) is provided in Figure 3.9 for FC-PFHS_Ref, FC-PFHS_Case4, and FC-PFHS_Case8.

The maximum and minimum temperature variations on the base plate for FC-PFHS_Ref, FC-PFHS_Case4, and FC-PFHS_Case8 are 3.48%, 4.95%, and 4.55%, respectively.

Maintaining uniform cooling performance is crucial to avoid the formation of local hot spots. Based on the size of the geometry and temperature distribution observed in this study, it can be concluded that uniform cooling has been successfully achieved.

CHAPTER 4

CONCLUSION AND FUTURE WORK

As technology advances, the demand for effective cooling of electronic components continues to grow. Traditional cooling methods are often unable to handle the increasing heat loads efficiently. Hence, there is a pressing need to explore new solutions to ensure optimal operation of electronic components. Metal foams emerge as promising candidates due to their high surface area-to-volume ratio, lightweight nature, and ability to significantly enhance heat transfer. However, increasing the surface area of the foam introduces the drawback of increasing pressure drop. Hence, it becomes crucial to determine an optimal threshold where hydrothermal performance remains favorable. Previous research extensively investigates the use of metal foams either as standalone heat sinks or in conjunction with pin fins. However, existing studies are confined by limited geometries in heat sink designs incorporating both foams and fins. In this study, a novel geometry has been devised to address this limitation. To assess the cooling performance of this novel configuration, experiments are conducted wherein aluminum foams are cladded onto pin fins on heat sinks. The experimental study involves the utilization of PFHS alongside two variations of FC-PFHSs featuring different PPI values. A comparative analysis is performed to evaluate the hydrothermal performance of these distinct geometries. Subsequently, a numerical model is developed and successfully validated using the experimental results. With the validated numerical model, a parametric analysis is carried out. This analysis focuses on exploring the impact of cladding thickness, with two varying thickness values. Additionally, considering the significance of porosity in foams, four different porosity values are studied for all distinct geometries. Ultimately, the study delves into a comprehensive discussion on the thermal and hydrothermal performance of these cases.

- During the experiments, it is observed that the addition of aluminum cladding enhances the hydrothermal performance of the heat sink. Both the 20 and 40 PPI FC-PFHSs exhibit superior hydrothermal performance compared to the unclad heat sink with identical outer diameter.
- Due to the inability to measure pressure drop in the experiments for the 40 PPI FC-PFHS, a comparison of the hydrothermal performance between the 20 and 40 PPI FC-PFHS is conducted using numerical model results. It is determined that the hydrothermal performance of the FC-PFHS_Ref surpassed that of the 40 PPI FC-PFHS.
- FC-PFHS_Ref exhibits superior thermal performance compared to the 40 PPI FC-PFHS and PFHS.
- 40 PPI FC-PFHS shows better thermal and hydrothermal performance relative to PFHS.
- A parametric study is conducted using 20 PPI FC-PFHSs, varying cladding thickness and porosity values. For the calculation of performance evaluation criterion (PEC), the base case is established with a 5mm diameter PFHS.
- As the diameter of the cladding increases, the thermal performance of the heat sink also increases. However, as the thickness of the cladding increases, the pressure drop experiences a tremendous increase which results in high pumping powers for the fan or pump used for cooling [38].
- Altering the porosity does not notably impact the thermal performance of the heat sink for the studied Re. However, it does lead to variations in the pressure drop values.
- All of the studied cases show an enhancement in hydrothermal performance. Among all twelve cases studied, 20 PPI 10 mm diameter FC-PFHS with a porosity value of 0.95 shows the best hydrothermal performance with an increase of 46.5% compared to the base case.

As future work, a new set of experiments may be designed in order to investigate the effect of employing various metal foams for cladding PFHSs, with corresponding numerical models developed accordingly. Additionally, given the challenge of measuring pressure drop for all cases in the current study, employing a new pressure transmitter capable of measuring low pressures could enhance future investigations.

An optimization study may be conducted for using different metal foams for claddings in terms of cost effectiveness. An optimization study could also explore whether utilizing metal foams for enhancing heat transfer justifies dealing with the associated high pumping power requirements. A better integration way of metal foams onto pin fins may be investigated without creating additional contact resistance between pin fins and metal foams. Different geometries can be created and studied both experimentally and numerically which could offer valuable insights for further enhancing heat sink performance.

REFERENCES

[1] Z. Zhang, X. Wang, and Y. Yan, “A review of the state-of-the-art in electronic cooling,” *e-Prime - Advances in Electrical Engineering, Electronics and Energy*, vol. 1. Elsevier Ltd, Jan. 01, 2021. doi: 10.1016/j.prime.2021.100009.

[2] C. T. DeGroot, A. G. Straatman, and L. J. Betchen, “Modeling forced convection in finned metal foam heat sinks,” *Journal of Electronic Packaging, Transactions of the ASME*, vol. 131, no. 2, pp. 0210011–02100110, Jun. 2009, doi: 10.1115/1.3103934.

[3] Z. He, Y. Yan, and Z. Zhang, “Thermal management and temperature uniformity enhancement of electronic devices by micro heat sinks: A review,” *Energy*, vol. 216, Feb. 2021, doi: 10.1016/j.energy.2020.119223.

[4] M. Pedram and S. Nazarian, “Thermal modeling, analysis, and management in VLSI circuits: Principles and methods,” *Proceedings of the IEEE*, vol. 94, no. 8, pp. 1487–1501, 2006, doi: 10.1109/JPROC.2006.879797.

[5] S. M. Sohel Murshed and C. A. Nieto de Castro, “A critical review of traditional and emerging techniques and fluids for electronics cooling,” *Renewable and Sustainable Energy Reviews*, vol. 78. Elsevier Ltd, pp. 821–833, 2017. doi: 10.1016/j.rser.2017.04.112.

[6] S. Racha, “Heat transfer augmentation for electronic cooling,” *American Journal of Applied Sciences*, vol. 9, no. 3, pp. 436–439, 2012.

[7] M. D. Shende and A. Mahalle, “Cooling of electronic equipments with heat sink: A review of literature,” *IOSR Journal of Mechanical and Civil Engineering*, vol. 5, no. 2, pp. 56–61, 2013, [Online]. Available: www.iosrjournals.org

[8] V. Bianco, M. De Rosa, and K. Vafai, “Phase-change materials for thermal management of electronic devices,” *Applied Thermal Engineering*, vol. 214, Sep. 2022, doi: 10.1016/j.applthermaleng.2022.118839.

[9] J. Li *et al.*, “Ultrathin, soft, radiative cooling interfaces for advanced thermal management in skin electronics,” *Science Advances*, vol. 9, 2023, [Online]. Available: https://www.science.org

[10] A. Bejan and G. A. Ledezma, “Thermodynamic optimization of cooling techniques for electronic packages,” *International Journal of Heat Mass Transfer*, vol. 39, no. 6, pp. 1213–1221, 1996.

[11] C. S. Sharma, M. K. Tiwari, B. Michel, and D. Poulikakos, “Thermofluidics and energetics of a manifold microchannel heat sink for electronics with recovered hot water as working fluid,” *International Journal of Heat and Mass Transfer,* vol. 58, no. 1–2, pp. 135–151, 2013, doi: 10.1016/j.ijheatmasstransfer.2012.11.012.

[12] C. S. Sharma, S. Zimmermann, M. K. Tiwari, B. Michel, and D. Poulikakos, “Optimal thermal operation of liquid-cooled electronic chips,” *International Journal of Heat and Mass Transfer*, vol. 55, no. 7–8, pp. 1957–1969, Mar. 2012, doi: 10.1016/j.ijheatmasstransfer.2011.11.052.

[13] H. T. Dhaiban and M. A. Hussein, “The optimal design of heat sinks: A review,” *Journal of Applied and Computational Mechanics*, vol. 6, no. 4, pp. 1030–1043, 2020, doi: 10.22055/jacm.2019.14852.

[14] R. Muthukumarn, R. Rathnasamy, and R. Karthikeyan, “Experimental Study of Performance of Pin Fin Heat Sink under Forced Convection,” *International Journal of Mechanical Engineering and Information Technology,* vol. 4, 2016.

[15] D. E. Metzger, C. S. Fan, and S. W. Haley, “Effects of Pin Shape and Array Orientation on Heat Transfer and Pressure Loss in Pin Fin Arrays,” *Journal of Engineering for Gas Turbines and Power, Transactions of the ASME,* vol.

106, pp. 252–257, 1984, [Online]. Available: http://www.asme.org/about-asme/terms-of-use

[16] C. L. Chapman, S. Lee, and B. L. Schmidt, “Thermal performance of an elliptical pin fin heat sink,” *Proceedings of 1994 IEEE/CHMT 10th Semiconductor Thermal Measurement and Management Symposium (SEMI-THERM)*, pp. 24–31, 1994.

[17] W. A. Khan, J. R. Culham, and M. M. Yovanovich, “The role of fin geometry in heat sink performance,” *Journal of Electronic Packaging, Transactions of the ASME*, vol. 128, no. 4, pp. 324–330, Dec. 2006, doi: 10.1115/1.2351896.

[18] H. Jonsson and B. Palm, “Experimental comparison of different heat sink designs for cooling of electronics,” *ASME Heat Transfer Division,* vol. 329, pp. 27–34, 1996.

[19] M. K. Chyu, “Heat transfer and pressure drop for short pin-fin arrays with pin-endwall fillet,” *Journal of Heat Transfer, Transactions of the ASME,* vol. 112, pp. 926–932, 1990, [Online]. Available: http://heattransfer.asmedigitalcollection.asme.org/

[20] J. S. Issa and A. Ortega, “Experimental measurements of the flow and heat transfer of a square jet impinging on an array of square pin fins,” *Journal of Electronic Packaging, Transactions of the ASME*, vol. 128, no. 1, pp. 61–70, Mar. 2006, doi: 10.1115/1.2160513.

[21] “What are cellular metals and metal foams?” Accessed: Nov. 10, 2023. [Online]. Available: http://www.metalfoam.net/

[22] “What is Aluminum foam?” Accessed: Jul. 25, 2023. [Online]. Available: https://ergaerospace.com/aluminum-foam-cell-structure-material/

[23] V. V Calmidi and R. L. Mahajan, “The effective thermal conductivity of high porosity fibrous metal foams,” *Journal of Heat Transfer, Transactions of the*

ASME, vol. 121, pp. 466–471, 1999, [Online]. Available: https://heattransfer.asmedigitalcollection.asme.org/

[24] C. Y. Zhao, T. Kim, T. J. Lu, and H. P. Hodson, "Thermal transport in high porosity cellular metal foams," *Journal of Thermophysics and Heat Transfer,* vol. 18, no. 3, pp. 309–317, 2004, doi: 10.2514/1.11780.

[25] W. H. Hsieh, J. Y. Wu, W. H. Shih, and W. C. Chiu, "Experimental investigation of heat-transfer characteristics of aluminum-foam heat sinks," *Int J Heat Mass Transf*, vol. 47, no. 23, pp. 5149–5157, Nov. 2004, doi: 10.1016/j.ijheatmasstransfer.2004.04.037.

[26] I. Kurtbas and N. Celik, "Experimental investigation of forced and mixed convection heat transfer in a foam-filled horizontal rectangular channel," *International Journal of Heat and Mass Transfer,* vol. 52, no. 5–6, pp. 1313–1325, Feb. 2009, doi: 10.1016/j.ijheatmasstransfer.2008.07.050.

[27] A. Tamayol and K. Hooman, "Thermal assessment of forced convection through metal foam heat exchangers," *Journal of Heat Transfer,* vol. 133, no. 11, 2011, doi: 10.1115/1.4004530.

[28] S. Mancin, C. Zilio, A. Diani, and L. Rossetto, "Air forced convection through metal foams: Experimental results and modeling," *Int J Heat Mass Transf*, vol. 62, no. 1, pp. 112–123, 2013, doi: 10.1016/j.ijheatmasstransfer.2013.02.050.

[29] A. Bhattacharya and R. L. Mahajan, "Finned metal foam heat sinks for electronics cooling in forced convection," *Journal of Electronic Packaging, Transactions of the ASME*, vol. 124, no. 3, pp. 155–163, Sep. 2002, doi: 10.1115/1.1464877.

[30] H. R. Seyf and M. Layeghi, "Numerical analysis of convective heat transfer from an elliptic pin fin heat sink with and without metal foam insert," *Journal of Heat Transfer,* vol. 132, no. 7, pp. 1–9, Jul. 2010, doi: 10.1115/1.4000951.

[31] S. S. Feng, J. J. Kuang, T. Wen, T. J. Lu, and K. Ichimiya, "An experimental and numerical study of finned metal foam heat sinks under impinging air jet cooling," *International Journal of Heat and Mass Transfer,* vol. 77, pp. 1063–1074, 2014, doi: 10.1016/j.ijheatmasstransfer.2014.05.053.

[32] S. K. Mohammadian and Y. Zhang, "Cumulative effects of using pin fin heat sink and porous metal foam on thermal management of lithium-ion batteries," *Applied Thermal Engineering,* vol. 118, pp. 375–384, 2017, doi: 10.1016/j.applthermaleng.2017.02.121.

[33] Y. Li, L. Gong, M. Xu, and Y. Joshi, "Hydraulic and thermal performances of metal foam and pin fin hybrid heat sink," *Applied Thermal Engineering,* vol. 166, Feb. 2020, doi: 10.1016/j.applthermaleng.2019.114665.

[34] Y. Li, L. Gong, M. Xu, and Y. Joshi, "Enhancing the performance of aluminum foam heat sinks through integrated pin fins," *International Journal of Heat and Mass Transfer,* vol. 151, Apr. 2020, doi: 10.1016/j.ijheatmasstransfer.2020.119376.

[35] J. Wang, H. Kong, Y. Xu, and J. Wu, "Experimental investigation of heat transfer and flow characteristics in finned copper foam heat sinks subjected to jet impingement cooling," *Applied Energy,* vol. 241, pp. 433–443, May 2019, doi: 10.1016/j.apenergy.2019.03.040.

[36] A. M. Ranjbar, Z. Pouransari, and M. Siavashi, "Improved design of heat sink including porous pin fins with different arrangements: A numerical turbulent flow and heat transfer study," *Applied Thermal Engineering,* vol. 198, Nov. 2021, doi: 10.1016/j.applthermaleng.2021.117519.

[37] S. S. Panse, P. Singh, and S. V. Ekkad, "Thermal hydraulic performance augmentation by high-porosity thin aluminum foams placed in high aspect ratio ducts," *Applied Thermal Engineering,* vol. 161, Oct. 2019, doi: 10.1016/j.applthermaleng.2019.114162.

[38] Y. Serkan Şahin, B. İsmet Toprak, İ. Solmaz, and Ö. Bayer, “Investigation of flow and heat transfer behavior of integrated pin fin-aluminum foam heat sink,” *Applied Thermal Engineering,* vol. 219, Jan. 2023, doi: 10.1016/j.applthermaleng.2022.119504.

[39] “Aluminum 6061-T6; 6061-T651.” Accessed: Nov. 12, 2023. [Online]. Available: https://asm.matweb.com/search/SpecificMaterial.asp?bassnum=ma6061t6

[40] H. Babar, H. Wu, H. M. Ali, and W. Zhang, “Hydrothermal performance of inline and staggered arrangements of airfoil shaped pin-fin heat sinks: A comparative study,” *Thermal Science and Engineering Progress*, vol. 37, Jan. 2023, doi: 10.1016/j.tsep.2022.101616.

[41] E. M. Sparrow, J. W. Ramsey, and C. A. C. Altemani, “Experiments on In-line Pin Fin Arrays-and Performance Comparisons with Staggered Arrays,” *Journal of Heat Transfer, Transactions of the ASME,* vol. 102, pp. 44–50, 1980.

[42] J. S. Park, K. M. Kim, D. H. Lee, H. Cho, and M. K. Chyu, “Heat transfer on rotating channel with various heights of pin-fin,” *Proceedings of ASME Turbo Expo 2008: Power for Land, Sea and Air*, 2008, [Online]. Available: http://www.asme.org/about-asme/terms-of-use

[43] M. K. Chyu, S. C. Siw, and H. K. Moon, “Effects of height-to-diameter ratio of pin element on heat transfer from staggered pin-fin arrays,” *Proceedings of ASME Turbo Expo 2009: Power for Land, Sea and Air,* 2009, [Online]. Available: http://www.asme.org/about-asme/terms-of-use

[44] O. N. Sara, “Performance analysis of rectangular ducts with staggered square pin fins,” *Energy Conversion and Management,* vol. 44, pp. 1787–1803, 2003, [Online]. Available: www.elsevier.com/locate/enconman

[45] “Duocel® Aluminum Foam Panel – 3″ x 3″.” Accessed: Aug. 10, 2023. [Online]. Available: https://www.duocelfoam.com/product/aluminum-foam-panel-3inch-x-3inch/

[46] P. Nithiarasu, K. N. Seetharamu, and T. Sundararajan, “Finite element modelling of flow, heat and mass transfer in fluid saturated porous media,” *Archives of Computational Methods in Engineering,* vol. 9, pp. 3–42, 2002.

[47] V. V Calmidi and R. L. Mahajan, “Forced Convection in High Porosity Metal Foams,” *Journal of Heat Transfer, Transactions of the ASME,* vol. 122, pp. 557–565, 2000, [Online]. Available: http://heattransfer.asmedigitalcollection.asme.org/

[48] M. S. Phanikumar and R. L. Mahajan, “Non-Darcy natural convection in high porosity metal foams,” *International Journal of Heat and Mass Transfer,* vol. 45, pp. 3781–3793, 2002, [Online]. Available: www.elsevier.com/locate/ijhmt

[49] K. C. Leong and L. W. Jin, “Effect of oscillatory frequency on heat transfer in metal foam heat sinks of various pore densities,” *International Journal of Heat and Mass Transfer,* vol. 49, no. 3–4, pp. 671–681, Feb. 2006, doi: 10.1016/j.ijheatmasstransfer.2005.08.015.

[50] T. M. Jeng and S. C. Tzeng, “Numerical study of confined slot jet impinging on porous metallic foam heat sink,” *International Journal of Heat and Mass Transfer,* vol. 48, no. 23–24, pp. 4685–4694, Nov. 2005, doi: 10.1016/j.ijheatmasstransfer.2005.06.032.

[51] A. Cavallini, S. Mancin, L. Rossetto, and C. Zilio, “Air flow in aluminum foam: Heat transfer and pressure drops measurements,” *Experimental Heat Transfer*, vol. 23, no. 1, pp. 94–105, Jan. 2010, doi: 10.1080/08916150903402765.

[52] “EPO-TEK ® H20E.” [Online]. Available: www.epotek.com

[53] Keysight Technologies, “N5700 Series System DC Power Supplies.” [Online]. Available: www.keysight.com

[54] Airflow, “TA-2 range of thermal anomemeters.”

[55] “Air differential pressure transmitter mps590.” Accessed: Oct. 23, 2023. [Online]. Available: http://mesens.com/Urun/Hava-Fark-Basinc-Transmiteri-MPS590

[56] Keysight Technologies, “E3640A-E3649A Programmable DC Power Supplies.”

[57] Keysight Technologies, “34972A LXI Data Acquisition / Data Logger Switch Unit.”

[58] “Differential Pressure Transmitter Explained”, Accessed: Nov. 09, 2023. [Online]. Available: https://www.realpars.com/blog/differential-pressure-transmitter#:~:text=How%20Does%20a%20DP%20Flow,more%20pressure%20drop%20is%20created.

[59] S. C. Tzeng and T. M. Jeng, “Convective heat transfer in porous channels with 90-deg turned flow,” *International Journal of Heat and Mass Transfer,* vol. 49, no. 7–8, pp. 1452–1461, Apr. 2006, doi: 10.1016/j.ijheatmasstransfer.2005.09.024.

[60] D. Bogojevic *et al.*, “Experimental investigation of non-uniform heating effect on flow boiling instabilities in a microchannel-based heat sink,” *International Journal of Thermal Sciences*, vol. 50, no. 3, pp. 309–324, Mar. 2011, doi: 10.1016/j.ijthermalsci.2010.08.006.

[61] T. Alam, P. S. Lee, C. R. Yap, and L. Jin, “Experimental investigation of local flow boiling heat transfer and pressure drop characteristics in microgap channel,” *International Journal of Multiphase Flow*, vol. 42, pp. 164–174, Jun. 2012, doi: 10.1016/j.ijmultiphaseflow.2012.02.007.

[62] A. Alhusseny, Q. Al-Aabidy, N. Al-Zurfi, A. Nasser, and M. Aljanabi, "Cooling of high-performance electronic equipment using graphite foam heat sinks," *Applied Thermal Engineering,* vol. 191, Jun. 2021, doi: 10.1016/j.applthermaleng.2021.116844.

[63] M. A. Alfellag, H. E. Ahmed, M. G. Jehad, and M. Hameed, "Assessment of heat transfer and pressure drop of metal foam-pin-fin heat sink," *International Journal of Thermal Sciences*, vol. 170, Dec. 2021, doi: 10.1016/j.ijthermalsci.2021.107109.

[64] L. Gong, Y. Li, Z. Bai, and M. Xu, "Thermal performance of micro-channel heat sink with metallic porous/solid compound fin design," *Applied Thermal Engineering,* vol. 137, pp. 288–295, Jun. 2018, doi: 10.1016/j.applthermaleng.2018.03.065.

[65] R. J. Moffat, "Describing the uncertainties in experimental results," *Experimental Thermal and Fluid Science,* pp. 3–17, 1988.

[66] "Thermocouple types." Accessed: Dec. 13, 2023. [Online]. Available: https://www.omega.com/en-us/resources/thermocouple-types#:~:text=Accuracy%3A%20Type%20T%20thermocouples%20have,per%20ANSI%2FASTM%20E230).

[67] Theodore L. Bergman, Adrienne S. Lavine, Frank P. Incropera, and David P. DeWitt, *Fundamentals of Heat and Mass Transfer*. Wiley, 2021.

[68] ANSYS, "Ansys Fluent Theory Guide," 2021.

[69] P. De Jaeger, C. T'Joen, H. Huisseune, B. Ameel, S. De Schampheleire, and M. De Paepe, "Assessing the influence of four bonding methods on the thermal contact resistance of open-cell aluminum foam," *International Journal of Heat and Mass Transfer,* vol. 55, no. 21–22, pp. 6200–6210, Oct. 2012, doi: 10.1016/j.ijheatmasstransfer.2012.06.043.